The Structures and Total (Minor + Major) Merger Histories of Massive Galaxies Up To Z# 3 in the Hst Goods Nicmos Survey: A Possible Solution to the Size Evolution Problem

Author(s):
Bluck, Asa F.L.; Conselice, Christopher J.; Buitrago, Fernando; Grützbauch, Ruth; Hoyos, Carlos; Mortlock, Alice; Bauer, Amanda E.

Publication date:
2012-03-01

Permanent link:
https://doi.org/https://doi.org/10.3929/ethz-b-000256400

Originally published in:
The Astrophysical Journal 747(1), https://doi.org/10.1088/0004-637x/747/1/34

The Astrophysical Journal, 747:34 (17pp), 2012 March 1 doi:10.1088/0004-637X/747/1/34

THE STRUCTURES AND TOTAL (MINOR + MAJOR) MERGER HISTORIES OF MASSIVE GALAXIES UP TO $z \sim 3$ IN THE *HST* GOODS NICMOS SURVEY: A POSSIBLE SOLUTION TO THE SIZE EVOLUTION PROBLEM

Asa F. L. Bluck[1], Christopher J. Conselice[2], Fernando Buitrago[2], Ruth Grützbauch[2], Carlos Hoyos[2], Alice Mortlock[2], and Amanda E. Bauer[3]

[1] Gemini Observatory, Northern Operations Center, Hilo, Hawaii 96720, USA; abluck@gemini.edu
[2] Centre for Astronomy and Particle Theory, School of Physics and Astronomy, University of Nottingham, Nottingham NG7 2RD, UK; conselice@nottingham.ac.uk
[3] Australian Astronomical Observatory, Epping, NSW 1710, Australia; abauer@aa0.gov.au
Received 2011 September 20; accepted 2011 December 12; published 2012 February 13

ABSTRACT

We investigate the total major (>1:4 by stellar mass) and minor (>1:100 by stellar mass) merger history of a population of 80 massive ($M_* > 10^{11}\,M_\odot$) galaxies at high redshifts ($z = 1.7$–3). We utilize extremely deep and high-resolution *Hubble Space Telescope H*-band imaging from the GOODS NICMOS Survey, which corresponds to rest-frame optical wavelengths at the redshifts probed. We find that massive galaxies at high redshifts are often morphologically disturbed, with a *CAS* (concentration, *C*; asymmetry, *A*; clumpiness, *S*) deduced merger fraction $f_m = 0.23 \pm 0.05$ at $z = 1.7$–3. We find close accord between close pair methods (within 30 kpc apertures) and *CAS* methods for deducing major merger fractions at all redshifts. We deduce the total (minor + major) merger history of massive galaxies with $M_* > 10^9\,M_\odot$ galaxies, and find that this scales roughly linearly with log-stellar-mass and magnitude range. We test our close pair methods by utilizing mock galaxy catalogs from the Millennium Simulation. We compute the total number of mergers to be $(4.5 \pm 2.9)/\langle\tau_m\rangle$ from $z = 3$ to the present, to a stellar mass sensitivity threshold of ~1:100 (where τ_m is the merger timescale in Gyr which varies as a function of mass). This corresponds to an average mass increase of $(3.4 \pm 2.2) \times 10^{11}\,M_\odot$ over the past 11.5 Gyr due to merging. We show that the size evolution observed for these galaxies may be mostly explained by this merging.

Key words: galaxies: evolution – galaxies: formation – galaxies: high-redshift – galaxies: interactions

Online-only material: color figures

1. INTRODUCTION

The cold dark matter paradigm for structure formation in the universe leads naturally to a hierarchical picture of galaxy growth, whereby large objects form from the merging together of smaller objects. As such, observing galaxies in a state of merging becomes desirable both as a probe of galaxy evolution and as a critical test of the ΛCDM cosmological model (see, e.g., Bertone & Conselice 2009). Many studies to date have probed the merger history of massive galaxies, in particular, up to high redshifts ($z < 3$); see, e.g., Patton et al. (2000), Conselice et al. (2003, 2007, 2009), Rawat et al. (2008), Bluck et al. (2009), Lopez-Sanjuan et al. (2010a, 2010b), and Lopez-Sanjuan et al. (2011).

At low to intermediate redshifts ($0 < z < 1.4$), close pair methods and morphological approaches find close accord in estimating the major merger history of massive galaxies (Bluck et al. 2009; Conselice et al. 2009). At the highest redshifts ($z > 1.5$), studies have concentrated primarily on close pair methods, as opposed to morphological approaches, due to restrictions on the resolution of imaging of very high redshift objects (Bluck et al. 2009). These studies find rough agreement in identifying a positive evolution of the major merger fraction with redshift, with an estimate for the most massive galaxies (with $M_* > 10^{11}\,M_\odot$) of evolution such that $f_m \propto (1+z)^{3.0\pm0.4}$, with no sign of this monotonic increase in merger fraction with redshift abating at higher redshifts (see Bluck et al. 2009, and similar results at lower redshifts in, e.g., Rawat et al. 2008; Bridge et al. 2010). For lower mass systems there is an observed peak in the merger fraction history at $z \sim 1$–2, as seen in Conselice et al. (2007), but to date no similar peak is observed for the most massive galaxies in the universe (with $M_* > 10^{11}\,M_\odot$), even out to $z = 3$. This disagrees with predictions from semianalytical interfaces with the Millennium Simulation, where a turnaround in merger fraction is expected for massive galaxies by $z \sim 2$ (Bertone & Conselice 2009). Interestingly, however, the merger rates computed in Bluck et al. (2009) agree comfortably with that predicted from the Millennium Simulation (Bertone & Conselice 2009). At some point the merger fractions must turn over, but this has yet to be observed or constrained for very massive galaxies.

The total number of major mergers that massive galaxies experience since $z \sim 3$ has been estimated assuming a merger timescale based on *N*-body simulations (see Lotz et al. 2008a, 2008b, 2010) as well as via an empirical measure (Conselice 2009), and a parameterization of the merger history (see Bluck et al. 2009 and Conselice et al. 2009). Current estimates suggest that the total number of major mergers (~1:4 by stellar mass) experienced since $z = 3$ by the most massive galaxies in the universe (with $M_* > 10^{11}\,M_\odot$) is $N_M = 1.7 \pm 0.5$ (Bluck et al. 2009). A similar result to this is found recently in Man et al. (2011) where the authors conclude that there are $N_M = 1.1 \pm 0.5$ major mergers over the same epoch. This implies that there is on average a mass increase of less than a factor of two or so directly due to major merging over the past 12 billion years of massive galaxy evolution. Additionally, there is a growing mass of evidence to suggest that over the same time period massive galaxies grow in effective radii by up to a factor of five by building up stellar matter in their outer regions (see, e.g., Trujillo et al. 2007; Buitrago et al. 2008; Cimatti et al. 2008; van Dokkum et al. 2009; Carrasco et al. 2010). To some extent spectroscopic measures of the velocity dispersions of a very small subset of these high-redshift massive galaxies are beginning to confirm that they are extremely dense and compact

(e.g., Cenarro & Trujillo 2009; Cappellari et al. 2009; Onodera et al. 2010).

If this growth in size is a real effect, and remains as dramatic as described currently in the literature, then a crucial question to address is: *How do these massive galaxies grow so much in size while growing relatively little in mass?* It is now thought that this growth is largely caused by adding stellar material to the outskirts of massive galaxies, such that the luminosity profiles grow in the outer regions of galaxies, leaving their cores predominantly unaffected (see Hopkins et al. 2009; Bezanson et al. 2009; van Dokkum et al. 2008, 2009; Buitrago et al. 2011). Doubtless, major merging will play a role in this growth, which is considered in this paper. However, it is also necessary to explore other possibilities, for example, alternative external influences such as minor mergers (also considered in this paper, Khochfar & Silk 2006, and Naab et al. 2009), cold gas inflow into the galaxies from the intergalactic medium inciting star formation (Dekel et al. 2009; Ceverino et al. 2010; C. J. Conselice et al. 2012, in preparation), and intrinsic evolution via, for example, active galactic nucleus (AGN) "puffing up" scenarios (e.g., Fan et al. 2008; Bluck et al. 2011). Although these AGN-driven models to provoke size evolution have been argued persuasively against recently (Trujillo et al. 2011) there is still a case to be made for the indirect effects of AGN redistributing gas around a massive active galaxy.

Low-mass galaxies which become integrated within massive galaxies through minor merging can give rise to a variety of triggers—i.e., igniting star formation and AGN activity, and potentially driving size evolution, as well as increasing the stellar mass of massive galaxies directly through adding stars. The merging process also changes the shape and peak of the mass and luminosity function of galaxies with cosmic time (see, e.g., Mortlock et al. 2011). Partly these triggers are caused by the fact that lower mass galaxies are often gas rich, and this influx of cool gas into massive galaxies can provide a source of fuel for AGN and material for star formation (e.g., Ricciardelli et al. 2010). This leads to the need to accurately probe the amount and nature of minor, as well as major, mergers a massive galaxy will experience during its evolution, which has until now been extremely difficult to achieve due to the limitations of depth and resolution of imaging galaxies at high redshifts.

In order to investigate the role of major and minor mergers, and structural evolution in massive galaxies, we combine a variety of different techniques and approaches. In this paper we analyze the structural and morphological properties, and minor merger fraction histories, for a sample of 80 massive ($M_* > 10^{11}\,M_\odot$) galaxies imaged in the rest-frame optical as part of the *Hubble Space Telescope* GOODS NICMOS Survey (*HST* GNS) at $1.7 < z < 3$ (see Conselice et al. 2011a). In particular, we compute the morphological *CAS* (concentration, *C*; asymmetry, *A*; clumpiness, *S*) parameters (Conselice et al. 2003) for our sample and use this to obtain an independent major merger fraction for our high-redshift sample of massive galaxies to compare with our close pair derived merger fraction in Bluck et al. (2009). We go on to compare the asymmetries (*A*; Conselice et al. 2003) of our massive galaxies with the residual flux fraction (RFF; Blakeslee et al. 2006) from their GALFIT fitting (first performed for our GNS galaxies in Buitrago et al. 2008). Furthermore, we exploit the exceptional resolution and depth of the *HST* GNS by using statistical close pair methods to investigate the minor merger history for these objects, constructing a minor merger history down to a mass sensitivity of ∼1:100 in stellar mass. This paper gives the first reliably measured total merger histories of massive galaxies over the majority of the age of the universe (over the past 12 billion years), and considers the question of whether or not merging can ultimately explain size evolution.

This paper is structured as follows. Section 2 describes the data used in this study, with Section 3 outlining our results in detail, including morphological and close pair analyses of our sample of high-redshift massive galaxies, and a full description of the methods used throughout this paper. Section 4 provides a discussion of our findings and considers the contribution to size evolution made by major and minor merging. Section 5 highlights our conclusions. Throughout the paper we assume a ΛCDM cosmology with $H_0 = 70\,\mathrm{km\,s^{-1}\ Mpc^{-1}}$, $\Omega_m = 0.3$, $\Omega_\Lambda = 0.7$, and adopt AB magnitude units.

2. DATA AND OBSERVATIONS

The *HST* GNS images a total of 8298 galaxies in the F160W (*H*) band, utilizing 180 orbits and 60 pointings of the *HST*/NICMOS-3 camera. These pointings are centered around massive galaxies at $1.7 < z < 3.0$, which are each observed to three orbits in depth. Each tile (with area $51\farcs2 \times 51\farcs2$ and pixel scale $0\farcs203\ \mathrm{pixel^{-1}}$) is observed in six exposures that combine to form images with a final pixel scale of $0\farcs1\ \mathrm{pixel^{-1}}$, and a point-spread function (PSF) of ∼0.″3 at FWHM. The total area of the survey is ∼43.7 arcmin^2. Limiting magnitudes reached are $H_{\mathrm{AB}} = 26.8\ (5\sigma)$ (see Conselice et al. 2011a).

The GNS is complete in stellar mass down to $M_* = 10^{9.5}\,M_\odot$ at $z = 3\sigma$–5σ, making it the largest mass complete sample of massive galaxies obtained to date at high redshifts ($z > 1.5$). The wealth of observational data available in the GOODS field allowed us to utilize data from the *U* to the *H* band in the determination of photometric redshifts. These are computed via a neural network approach, where spectroscopic redshifts in the field are used to train our codes. Multi-color stellar population fitting techniques were utilized with a Chabrier initial mass function to estimate stellar masses to an accuracy of ∼0.2–0.3 dex. The issue of thermally pulsating asymptotic giant branch stars in model spectral energy distribution (SED) fits for massive high-redshift galaxies was explored in detail in Conselice et al. (2007) and found not to be a significant problem for our stellar mass determination, perhaps increasing the errors to ∼0.3 dex, at the upper end of our initial estimation, which is still comfortably within the tolerance required for the analyses presented in this paper. More information on the GNS can be found in Buitrago et al. (2008), Bluck et al. (2009, 2011), Grützbauch et al. (2011a, 2011b), and Mortlock et al. (2011), and a complete account, incorporating full details on the data acquisition and analysis, and a link to freely access our preliminary data products including tables and images in Conselice et al. (2011a). This paper provides full details on the sample selection, observations, source extraction, data catalogs, and determination of photometric redshifts, rest-frame colors, and stellar masses.

The initial galaxy selection, of the 80 extremely massive galaxies at $z = 1.7$–3 studied in detail in this paper, was designed to detect as much as possible all massive galaxies regardless of the age of their stellar populations, dust obscuration, star formation, or nuclear activity. The full details of this selection are provided in Section 2.2 of Conselice et al. (2011a). To summarize, a variety of techniques were used including color-selection methods, e.g., distant red galaxies (Franx et al. 2003; Papovich et al. 2006), Infrared Array Camera extremely red objects (Yan et al. 2004), and *BzK* color-selected galaxies (Daddi

et al. 2004, 2007). In addition to these color-selected methods we also utilize catalogs of Lyman-break-selected BM/BX objects and high-redshift dropout submillimeter galaxies, the intention being to optimize the total number of massive galaxies in the GNS. We then compute the stellar masses of these galaxies again using the NICMOS *H*-band + ACS optical bands to confirm the high stellar mass of these systems.

A discussion of more robust error estimates on stellar masses can be found in Bluck et al. (2009), where it is concluded, through Monte Carlo simulation, that systematic errors arising out of Poisson errors from the steepness of the stellar mass function (Eddington bias) do not result in a significant infiltration of lower mass objects. Moreover, even if some lower mass galaxies do enter our sample they must have very similar merger properties to the genuinely very massive galaxies. Further discussion on the use of the SExtractor package to produce galaxy catalogs is also provided in Bluck et al. (2009) and in Conselice et al. (2011a), with special concern for deblending accuracy and removal of stellar objects and spurious detections. In essence, point-like (non-extended) sources were removed and later objects without galaxy-like colors were removed. This is, of course, vital to achieve well when utilizing close pair statistics approaches. For our sample of massive galaxies, each image was looked at carefully by eye and the source extraction parameters were deduced by optimizing deblending accuracy.

By way of comparison to lower redshift data, we utilize the Palomar Observatory Wide-field InfraRed (POWIR) survey (PI: C. J. Conselice) throughout this paper. Full details of this can be found in Conselice et al. (2007).

3. RESULTS

3.1. CAS Morphologies

Morphology is one of the oldest methods used for analyzing the properties of galaxies (see back to, e.g., Hubble 1926). However, it is certainly not without its difficulties and controversies. The need for automated (computational) approaches which are not influenced by subjective observer biases and assumptions has been profoundly lacking throughout much of the history of astronomy, as well as the need for a way to categorize the morphologies of galaxies in a model-independent way. One of the recent attempts to address both of these problems is the *CAS* structural parameters designed by Conselice et al. (2003). These offer a physically motivated, non-parametric, and computational scheme to uniquely position galaxies in a three-dimensional structural space dependent on the concentration, asymmetry, and clumpiness of their light profiles. The basic assumption is that galaxies contain information about their natures and histories embedded within their structures, and furthermore that those structures are, or can be, revealed by their observed two-dimensional spatial distribution of optical light.

Using our data the clumpiness parameter (*S*) is incalculable due to limitations in the resolution of our images (of PSF $\sim 0\farcs3$). As such, we constrain our analysis here to the *C*–*A* plane (or concentration–asymmetry plane), where these parameters require less high spatial resolution and are in general affected much less by redshift effects. *C* and *A* are defined in full detail in Conselice et al. (2009), as well as early definitions in Conselice et al. (2003). For the purposes of this paper it should be sufficient to comment that *A* is a measure of the total global asymmetry of a galaxy, based on minimizing the total residual left from subtracting a 180° rotation from the original galaxy image by allowing the center of rotation to vary within the code (Conselice et al. 2003). A high numerical value of *A* indicates a large global asymmetry. *C* is a probe of the concentration of the light distribution and in particular is constructed from the logarithm of the ratio of the radii at which 80% and 20% of the light of the entire galaxy (to the Petrosian radius) is contained. Higher values of *C* indicate more concentrated light profiles.

The structural data for our sample of high-redshift massive galaxies is presented in Table 1. We plot relative frequency histograms of the computed *C* and *A* parameters for our high-redshift GNS massive galaxies (overplotting the histograms for the lower redshift Extended Groth Strip (EGS) massive galaxies by way of comparison) in Figure 1. We plot where these massive galaxies lie in *C*–*A* space in Figure 2. We find that there is evolution with cosmic time such that massive galaxies become more concentrated and less asymmetric (to 5σ and 4σ confidence, respectively) at lower redshifts. The evolution in asymmetry will be considered in detail in the subsequent sections (especially in relation to inferred morphologically determined merger fractions), but it is a quantitative reiteration of the qualitative results found in, for example, Forster-Schreiber et al. (2011) and Elmegreen et al. (2011) whereby massive galaxies at higher redshifts are more frequently irregular and clumpier than their low-redshift counterparts. The evolution in concentration is reflective of a tendency for higher redshift massive galaxies to have low Sérsic indices and hence exhibit preferentially disk-like structures. This is considered fully in Buitrago et al. (2011) and is also alluded to in Weinzirl et al. (2011). Presumably, the major merging experienced by these massive galaxies serves to raise their Sérsic indices, through transforming rotationally supported spirals into kinematic-pressure supported ellipticals via an irregular or morphologically disturbed and kinematically chaotic phase.

Different morphologies of galaxies separate convincingly in the three-dimensional *C*–*A*–*S* space in the local universe, with the most significant division for this paper being the region where major merging galaxies tend to reside. It should be noted here that *CAS*-measured merger fractions (such as those presented in the following sections) are only sensitive to major merging of >1:4 by stellar mass (Conselice 2006; Lotz et al. 2008a, 2008b). The applicability of these methods to higher redshifts is considered for the case of identifying major merging systems in the following subsection. Also in Section 3.1.2 we explore the *CAS*-determined major merger history of massive galaxies in detail.

In the near future these methods can be applied to Wide Field Camera 3 images from the *HST* with greater reliability and the potential to compare across different wavebands (see, e.g., Conselice et al. 2011b). We do not explore the morphologies of the *HST* Advanced Camera for Surveys (ACS) images of our galaxies, even though they are of higher resolution than our NICMOS imaging, for two reasons. First, the ACS imaging is in the rest-frame UV for the redshifts of our galaxies and hence not representative of the underlying established stellar populations' light profiles. Therefore, it is not useful for commenting on global asymmetry, as it is dominated by knots of star formation (e.g., Pannella et al. 2009), and second, although most of our population of galaxies are visible in the ACS, many of these show up as point sources or very faint extended sources only (see Conselice et al. 2011a). This is most probably due to our sample of massive galaxies having high dust obscuration (see Bauer et al. 2011). These issues emphasize the need for near-infrared study of massive galaxies at high redshifts due to the lack of information acquirable about their established (older)

Table 1
GNS Massive Galaxies: Structural and Close Pair Data

GNS ID	R.A.	Decl.	$z_{\rm phot}$	Log(M_* [$M_\odot$])	$N_{\rm MP,corr}$	$N_{\rm TP,corr}$	C	A
21	189.1354	62.1172	2.70	11.05	0.00	0.02	2.6	0.26
43	189.1254	62.1155	2.20	11.08	0.00	0.00	3.1	0.35
77	189.1326	62.1121	1.91	11.41	0.00	0.00	2.7	0.19
227	189.1198	62.1355	2.07	11.20	0.00	0.03	3.1	0.27
373	189.0587	62.1635	2.51	11.06	1.39	0.50	2.6	0.24
552	189.0772	62.1510	1.93	11.33	0.00	1.42	2.9	0.20
730	189.2512	62.1527	2.47	11.09	0.00	0.00	2.5	0.31
840	189.1737	62.1673	1.93	11.30	0.00	0.97	2.7	0.17
856	189.1788	62.1663	1.74	11.38	0.00	0.00	3.2	0.37
999	189.1430	62.2335	1.98	11.17	0.00	0.00	2.2	0.27
1129	189.5074	62.2717	2.37	11.19	0.00	0.00	2.9	0.40
1144	189.5035	62.2700	2.07	11.13	0.00	0.00	2.9	0.25
1257	189.2264	62.2922	2.02	11.00	0.00	0.46	2.4	0.30
1394	189.3997	62.3453	2.04	11.36	0.00	0.00	2.8	0.20
1533	189.3058	62.1791	2.56	11.13	1.75	3.02	3.0	0.27
1666	189.2567	62.1962	2.36	11.38	0.73	0.22	2.5	0.24
1769	189.2737	62.1871	1.95	11.32	1.59	0.00	3.5	0.45
1826	189.0732	62.2613	2.20	11.28	0.51	1.17	2.3	0.32
1942	189.2777	62.2546	2.51	11.03	1.65	0.88	2.6	0.32
2049	189.3130	62.2047	2.40	11.21	1.25	1.30	2.3	0.34
2066	189.3002	62.2034	2.80	11.35	1.21	2.21	2.6	0.30
2083	189.3122	62.2016	2.72	11.28	0.44	0.43	2.3	0.38
2282	189.3069	62.2626	2.30	11.13	0.00	0.00	2.5	0.40
2411	189.0479	62.1761	2.10	11.17	0.00	0.00	2.3	0.15
2564	189.2110	62.2488	1.83	11.13	0.00	0.00	2.7	0.43
2678	189.0475	62.1486	2.50	11.53	0.58	0.00	0.0	0.42
2734	189.0423	62.1463	2.60	11.03	0.00	0.07	1.2	0.14
2764	189.0525	62.1433	2.20	11.15	0.00	0.00	2.5	0.26
2837	189.0944	62.2750	2.30	11.39	0.37	1.61	3.0	0.27
2902	189.0913	62.2677	2.00	11.22	0.00	0.00	2.8	0.34
2965	189.0799	62.2449	2.80	11.13	0.25	1.29	2.7	0.29
3036	189.0869	62.2377	2.10	11.11	0.57	1.84	1.9	0.48
3126	189.1304	62.1661	2.10	11.09	0.00	0.42	2.9	0.36
3250	189.2291	62.1385	2.30	11.12	0.00	0.00	2.5	0.29
3387	189.2942	62.3472	1.83	11.01	0.47	0.00	2.3	0.41
3422	189.2808	62.3442	2.80	11.09	0.00	0.00	2.4	0.27
3582	189.0987	62.1693	2.40	11.18	0.00	0.00	3.4	0.35
3629	189.1829	62.2725	2.10	11.28	1.69	2.11	2.6	0.25
3766	189.2056	62.3226	2.10	11.19	0.00	0.00	2.5	0.29
3818	189.2022	62.3171	1.75	11.41	0.77	0.00	3.4	0.27
3822	189.2198	62.3169	2.20	11.06	0.00	0.00	2.9	0.16
3970	189.3319	62.2059	2.34	11.16	0.40	0.45	2.9	0.33
4033	189.4641	62.2440	2.07	11.04	0.74	1.20	2.7	0.30
4121	189.4564	62.2332	1.92	11.20	0.00	0.07	2.4	0.60
4239	188.9812	62.1738	2.20	11.17	0.00	0.00	2.7	0.23
4282	53.0938	−27.8013	2.60	11.08	0.00	1.07	2.9	0.35
4301	53.0923	−27.8031	2.40	11.33	0.00	0.00	2.3	0.21
4353	53.1011	−27.8086	1.97	11.21	0.00	0.00	2.7	0.22
4400	53.1013	−27.7117	2.30	11.10	0.73	0.16	2.8	0.23
4434	53.0976	−27.7153	2.14	11.06	0.54	0.00	2.7	0.30
4557	53.0892	−27.7601	2.27	11.21	0.65	0.02	2.8	0.27
4706	53.1231	−27.8033	2.35	11.10	0.00	0.00	2.8	0.31
4754	53.1200	−27.8082	2.00	11.50	0.00	0.00	2.4	0.20
4882	53.1718	−27.8257	1.74	11.10	0.00	0.00	2.7	0.33
4941	53.2300	−27.8508	1.83	11.01	0.00	0.00	0.0	0.00
5171	53.0632	−27.6997	2.40	11.01	0.00	0.00	2.3	0.36
5282	53.0860	−27.7096	2.10	11.09	0.00	1.02	2.8	0.24
5372	53.1255	−27.8864	2.90	11.08	0.00	0.00	2.2	0.37
5445	53.1245	−27.8932	2.50	11.45	0.10	0.17	2.5	0.35
5524	53.1333	−27.9029	2.58	11.17	0.00	0.00	2.4	0.40
5533	53.1289	−27.9037	2.79	11.10	0.00	1.06	2.4	0.27
5764	53.2252	−27.8738	2.65	11.27	0.00	0.00	2.9	0.40
5853	53.0507	−27.7138	2.41	11.44	2.10	0.31	3.1	0.12
5933	53.0542	−27.7217	2.30	11.26	0.30	0.00	2.9	0.43
6035	53.0555	−27.8739	1.90	11.32	0.00	0.11	3.2	0.31
6114	53.0656	−27.8788	2.24	11.11	0.69	1.04	2.8	0.22

Table 1
(Continued)

GNS ID	R.A.	Decl.	z_{phot}	Log(M_* [$M_\odot$])	$N_{MP,corr}$	$N_{TP,corr}$	C	A
6220	53.0716	−27.8436	1.90	11.01	0.55	0.00	2.7	0.16
6352	53.0773	−27.8596	1.96	11.08	0.00	0.00	2.7	0.14
6468	53.1385	−27.6718	2.80	11.45	0.36	0.00	2.6	0.16
6575	53.0355	−27.6901	2.50	11.41	0.00	0.00	2.5	0.29
6584	53.0260	−27.6909	2.20	11.52	0.00	0.00	2.9	0.27
6584	53.0261	−27.6910	1.99	11.07	0.00	0.00	2.9	0.25
6876	53.0400	−27.6852	2.50	11.45	0.34	0.00	2.5	0.29
7090	53.0578	−27.8335	2.70	11.68	0.00	0.00	3.1	0.24
7156	53.1178	−27.9109	2.69	11.17	0.00	0.00	3.9	0.13
7321	53.1161	−27.8719	2.07	11.00	0.00	0.00	2.7	0.31
7425	53.1272	−27.8345	1.81	11.22	0.00	0.00	2.9	0.27
7677	53.1830	−27.7090	1.76	11.57	0.00	0.00	3.4	0.34
7970	53.0282	−27.7788	2.30	11.15	0.00	1.61	2.2	0.24
8140	53.1410	−27.7667	1.91	11.22	0.00	0.00	2.9	0.26
8214	53.1623	−27.7121	2.14	11.16	0.64	0.01	2.9	0.31

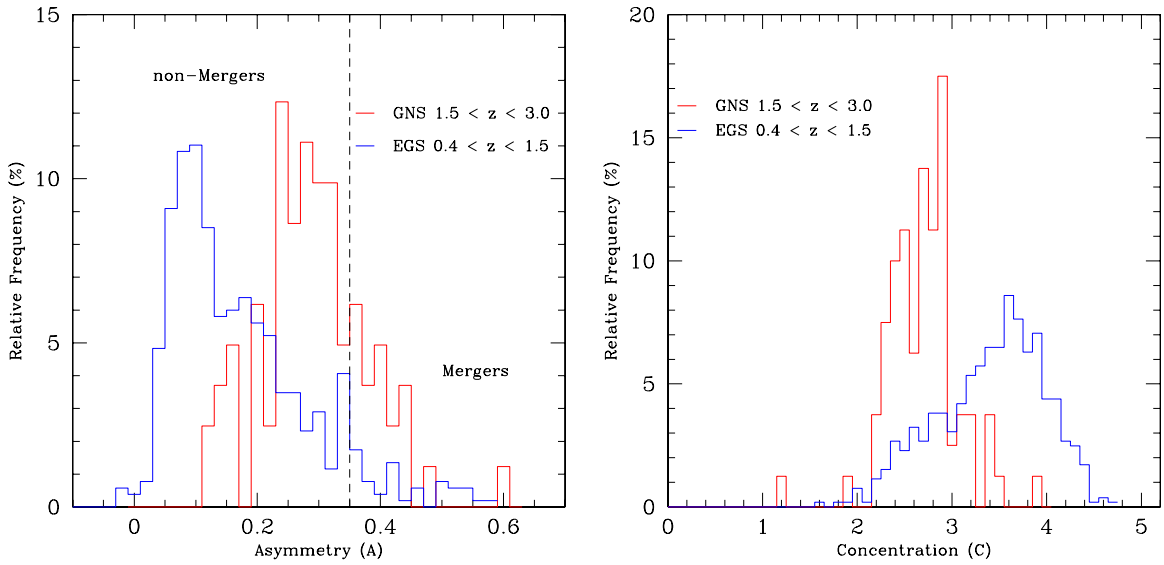

Figure 1. Relative frequency histograms for the asymmetry (A, left) and concentration (C, right) parameters. The red (light) histogram is for the high-redshift GNS sample of 80 massive ($M_* > 10^{11}\ M_\odot$) galaxies at $z = 1.7$–3 taken from the GNS. The blue (dark) histogram is for a comparison set of 524 massive ($M_* > 10^{11}\ M_\odot$) galaxies at intermediate redshift ($z = 0.4$–1.5) taken from ACS imaging of POWIR galaxies. There is evolution of the mean asymmetry from $\langle A \rangle = 0.290 \pm 0.010$ at $z \sim 2.5$ to $\langle A \rangle = 0.180 \pm 0.006$ at $z \sim 1$, indicating a 4σ difference from a K-S test. There is evolution in the mean concentration from $\langle C \rangle = 2.70 \pm 0.04$ at $z \sim 2.5$ to $\langle C \rangle = 3.40 \pm 0.02$ at $z \sim 1$, indicating a 5σ difference from a further K-S test. The errors quoted are the standard error on the mean. Also indicated on the left-hand plot are the regions where merging and non-merging galaxies tend to reside for $S < A$ systems.

(A color version of this figure is available in the online journal.)

stellar populations in the observed optical, hence rest-frame UV at $z = 1.5$–3. For now, our NICMOS imaging is the best available for this task.

3.1.1. Using CAS at High Redshifts

Regions within the C–A–S space were found to contain almost exclusively certain specific morphological types, e.g., late-type galaxies occupy a distinct region of the C–A plane. These distinctions, however, are drawn for local ($z \sim 0$) galaxies and their extension to the high-redshift universe must be taken with care. Much previous work has already looked into this problem, most notably Conselice et al. (2008) and Conselice et al. (2009). As discussed briefly above, it was concluded that the clumpiness parameter (S) is in principle very difficult to compute at high redshifts due to spatial resolution. The concentration (C) and asymmetry (A) parameters are much more robust at high redshift, but may still contain possible systematic offsets from their true (local) values. Much of the issues associated with using *CAS* at high redshifts are accounted for if one is careful to study equivalent rest-frame wavelengths, as done throughout this paper. Nonetheless, we run a set of simulations to test possible systematic effects from using *CAS* at high redshifts.

Our simulations take a broad variety of local universe galaxy types, from elliptical to irregular galaxies via a range of spirals. We then simulate how these galaxies would appear in the GNS by degrading the background to the noise level observed in the GNS and dimming the surface brightness in accord with the redshift. The *CAS* code is then run on both the original image and the artificially simulated high-redshift image and any differences are noted. From this analysis we conclude that there is a profound tendency for S to be underestimated at high redshifts, but that the concentration, C, and asymmetry, A, parameters recover a mean value comfortably within 2σ errors on the *CAS* code of the original value, where the morphological

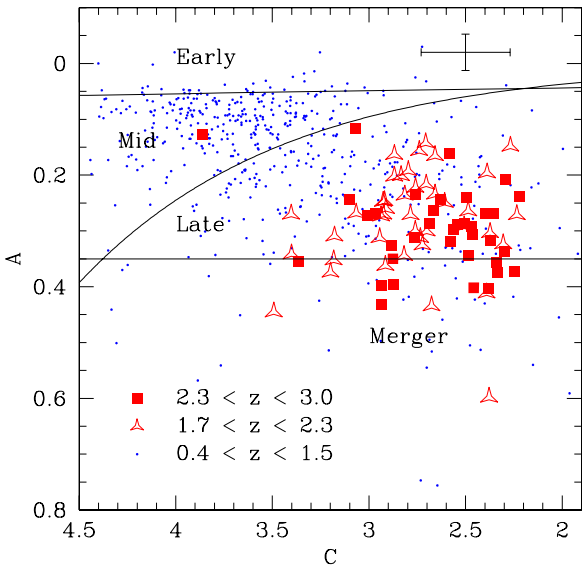

Figure 2. Asymmetry (A) plotted against concentration (C) for the 80 massive ($M_* > 10^{11}\ M_\odot$) galaxies in our sample at $1.7 < z < 3$. The data are divided via redshift, as described on the plot, and the regions where different morphologies reside at $z = 0$ are also marked on the plot. The placing of almost all non-merging galaxies in the "late-type" regime for the two higher redshift ranges is most probably an effect of all of these galaxies having some morphological disturbance (most likely via minor and sub-major merging), and should not be taken too seriously as a morphological classification, since these lines are drawn for $z = 0$ galaxies. The lowest redshift points (in blue) are taken from the EGS, whereas the higher redshift (red) points are taken from the GNS. The error bar displayed represents the average 1σ errors on the C and A parameters from the *CAS* code (Conselice et al. 2003).

(A color version of this figure is available in the online journal.)

K-correction is negligible as in the GNS because we view the rest-frame optical throughout.

These simulations are, however, limited in that they assume no surface brightness evolution of galaxies with cosmic time, which is known to be false; however, attempts to fully include this are beyond the scope of this first attempt, and moreover should serve to only increase the fidelity of the approach as it would result in brighter (and more easily visible) structures in the light profile at earlier times. There was a slight systematic tendency to underestimate A at high redshifts, but this was only observed at approximately the 1σ level or below. No similar systematic effect with concentration was noted.

One cause of this possible systematic high-redshift effect may be to lower the observed asymmetry (A) due to increased background noise; however, our own analysis through simulations of this effect are at best inconclusive. We find that there is perhaps a slight systematic trend to underestimate asymmetry values at high redshifts even after care has been taken to compare equivalent rest-frame wavelengths. Therefore, to be secure in our conclusions it is advisable to treat our A values as potential lower estimates at high redshifts, whereas to measure an A value *higher* than its true value at high redshifts would be very difficult to achieve. This is intuitive because the low spatial frequency light that A is most sensitive to is smoothed by surface brightness dimming. Future work on interpreting *CAS* at high redshift is needed, but what follows in this paper is a cautious first attempt, motivated and bolstered by early successes in simulation, and tethered by comparison to other tested methods, i.e., close pairs. Furthermore, the fact that we observe a primary result (that of high-redshift massive galaxies being more asymmetric than their local universe counterparts) in opposition to the dominant systematic effect implies that our conclusions must be robust regardless of this possible systematic.

3.1.2. Major Merger Fraction from CAS Morphology

The classic rest-frame optical definition for a *CAS*-selected major (>1:4 by stellar mass) merger is (see Conselice 2003; Conselice et al. 2009)

$$A > 0.35 \quad \text{and} \quad A > S. \tag{1}$$

That is, a major merging system will have an asymmetry in excess of $A = 0.35$, and furthermore an asymmetry in excess of its clumpiness, S. This selection has a proven track record of cleanly finding major mergers in the local universe at least (see Conselice 2003; de Propris et al. 2007). At higher redshifts there are some additional complications (see Section 3.1.1 and Conselice et al. 2009 for a full discussion). Ultimately, the effect of limitations in the resolution of imaging with the *HST*/NIC-3 camera (PSF $\sim 0\farcs3$) significantly reduces our sensitivity to the high-frequency clumpiness signal in very distant galaxies, in practice setting all S values more or less to zero. This means that the second criterion is irrelevant in practice as if $A > 0.35$ it is always greater than S at high z. This ensures that the asymmetry is a global property of the galaxy and not a result of, for example, clumpy star formation.

Furthermore, because we observe rest-frame V to B band with our *HST*/NICMOS H-band images at $z = 1.7$–3, we are probing the visible light and hence stellar population of the galaxies in question, not predominantly star formation as in many other high-redshift studies, which frequently view similar high-mass high-redshift objects in optical light, which corresponds to rest-frame UV. For a comparison of some of our galaxies in the NICMOS H band to ACS z band, see Figure 3 in Conselice et al. (2011a). Our massive high-z galaxies are much more clearly visible, with more prominent features, in the H band, whereas the ACS data are much more difficult to use for morphological classification. The most probable explanation for this is that our sample of massive high-z galaxies is highly dust obscured, see Bauer et al. (2011), as well as having a range of star formation rates. The rest frame UV is much more sensitive to knots of patchy star formation and indeed to dust regions causing obscuration than the rest-frame optical. Thus, we have very high resolution imaging (from *HST*) and additionally see the established stellar population (not star formation) via observing in the near-infrared, making the *HST* GNS an ideal survey to probe the structures and morphologies of high-redshift massive galaxies. More details on the SEDs of these galaxies are available in Bauer et al. (2011), as well as in Conselice et al. (2011a) and Grützbauch et al. (2011a, 2011b).

We identify 18 out of 80 massive galaxies that fit the empirical definition of a *CAS*-selected morphologically determined major merger, resulting in a total major merger fraction of $f_M(CAS) = 0.23 \pm 0.05$ at $1.7 < z < 3$. We further divide this redshift range up into two as in Bluck et al. (2009) to derive a merger fraction of $f_M(CAS) = 0.19 \pm 0.065$ (8 out of 43 galaxies) at $1.7 < z < 2.3$, and $f_M(CAS) = 0.27 \pm 0.08$ (10 out of 37 galaxies) at $2.3 < z < 3$. These values are plotted alongside the close pair derived merger fractions for the same galaxies, and the close pair + *CAS* merger fractions for lower redshift galaxies (from the POWIR Survey; see Conselice et al. 2007) in Figure 3. Here we add our latest morphologically determined major merger fractions to the merger fraction history plot of Bluck et al. (2009), noting that there is close agreement (to within the 1 σ errors) between *CAS*

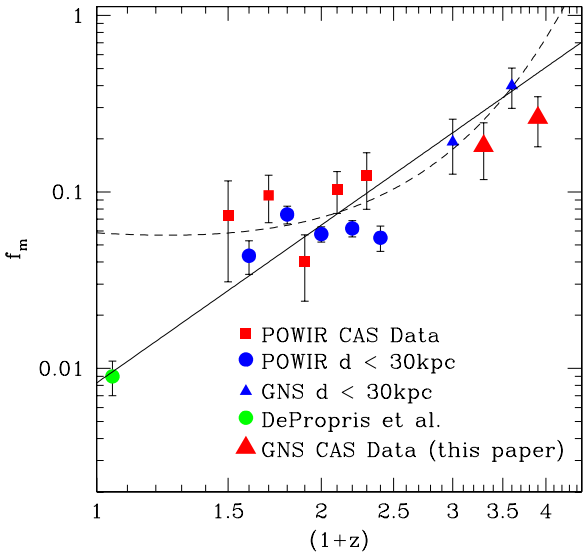

Figure 3. Major merger (f_m) evolution with redshift for massive ($M_* > 10^{11}\ M_\odot$) galaxies. This plot utilizes data from Bluck et al. (2009) and Conselice et al. (2007), where the major merger history of massive galaxies is probed using statistical close pair methods (at all z) and *CAS* morphologies (at $z < 1.5$). In this paper we add the *CAS* morphology determined major merger fractions for the two highest redshift ranges, up to $z = 3$ (large red triangles). There is generally good agreement between *CAS*-selected mergers and statistically determined close pairs (with $d < 30$ kpc) at all redshifts. Furthermore, both methods agree that there is a rise in merger fraction with redshift, which is parameterized here by a simple power-law best fit (solid line, with exponent $= 3 \pm 0.5$) and power-law exponential (dotted line); see Bluck et al. (2009; Figure 1) for further details on the fits. All displayed error bars are 1σ Poisson errors on the statistical counting.

(A color version of this figure is available in the online journal.)

and close pair ($d < 30$ kpc) major merger fractions at all redshift ranges probed, including at $z \sim 3$. This indicates that both approaches are sensitive to the underlying major merger history, with similar detection/merging timescales (see Conselice et al. 2009 for a detailed discussion of this issue). However, it should be emphasized that this is an agreement in computing the total number of mergers, not a correspondence of the approaches in identifying the same galaxies. *CAS* identifies *ongoing* major mergers, with the close pair method identifying likely *future* mergers. They are in general different populations with some small (∼15%) overlap. See Figure 4 for typical examples of *CAS*-selected major mergers.

Furthermore, we witness a modest rise in the merger fraction from morphologies of 8% (with $\sim 1\sigma$ significance) between our two highest redshift ranges, and note that this is only slightly smaller than the observed $\sim 2\sigma$ increase observed in Bluck et al. (2009) through close pair methods for the same galaxy population. It is possible that at our highest redshift range we are experiencing a systematic effect that effectively smooths our galaxies' light, thus underestimating A slightly. For now it is sufficient to note that broadly speaking there is agreement between close pair and *CAS* methods of determining major merger fractions, and that in both schemes there is a very high chance (4σ rise in f_m from $z = 0$ to $z = 3$ in both *CAS* and close pair methodologies) that the major merger fraction of massive galaxies was considerably higher at high redshifts than in the local universe (as shown in Figure 3). At lower redshifts (where there are numerous major merger fraction results for massive galaxies in the literature) our work agrees closely with many other studies using a variety of approaches from close pair statistics to morphologies, including Rawat et al. (2008), Jogee et al. (2009), Conselice et al. (2009), Bridge et al. (2010), and Lopez-Sanjuan et al. (2010a, 2010b). The highest redshift ranges probed here are the first such morphological measurements to the authors' knowledge, but recent complementary results in agreement with these have been presented in Man et al. (2011) using a statistical approach similar to Bluck et al. (2009).

3.1.3. A Link between Asymmetry (A) and GALFIT Residual Flux Fraction (RFF)

The true advantage of non-parametric computational techniques in fitting galaxy stellar light profiles over parametric techniques (such as Sérsic index fitting) is in the fact that no mathematical function is assumed to be appropriate for any given galaxy. In the cases of spheroidal or disk-like systems, fitting with Sérsic indices can be hugely advantageous (see, e.g., Peng et al. 2002; Trujillo et al. 2007; Buitrago et al. 2008),

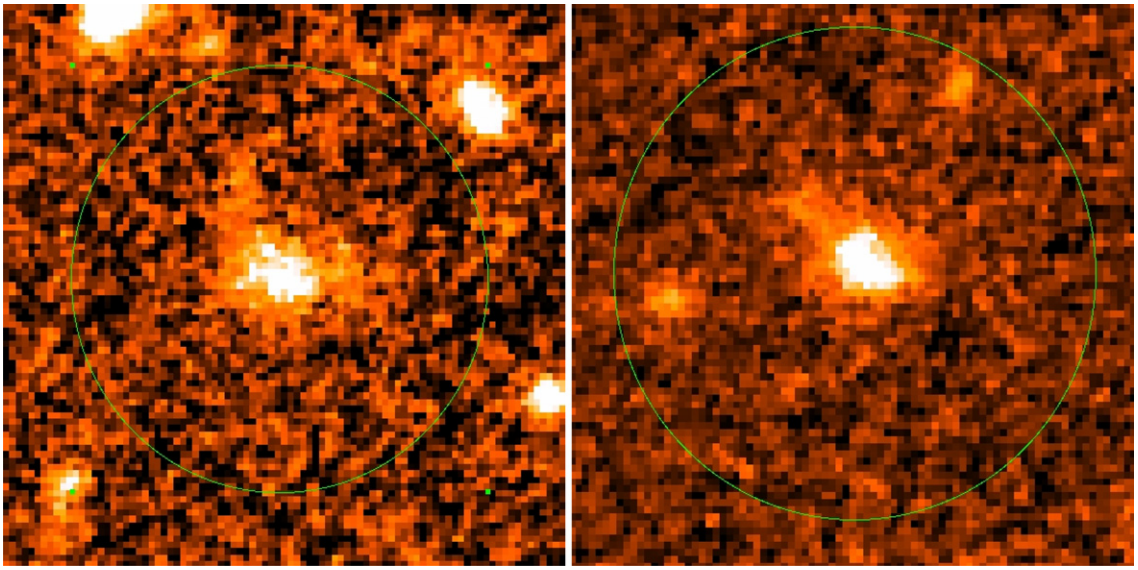

Figure 4. Typical examples of *CAS* major mergers: $A > 0.35$. *HST*/NICMOS H_{160} image of GNS-2282 (left) and GNS-3126 (right). The green circle indicates the $d < 30$ kpc (in physical units) region we use to select close pairs within.

(A color version of this figure is available in the online journal.)

but for morphologically disturbed or irregular galaxies this is certainly not the case. It is probable that highly asymmetric galaxies (those with a high A) will be poorly fit by GALFIT and other procedures for determining a Sérsic index. An excellent measure of the poorness of parametric fitting in the Sérsic index case is the RFF (Blakeslee et al. 2006). Thus, we hypothesize that there might be some correlation between RFF and A. If this is so, we will have better demarcated the applicability of parametric and non-parametric techniques when applied to fitting galaxies. Moreover, this will provide additional evidence that a high fraction of our massive galaxies at high-z are in fact morphologically disturbed.

Our samples of massive galaxies have previously had their light profiles fitted with a Sérsic index approach using the GALFIT package (see Peng et al. 2002). Early results concerning the size evolution of massive galaxies and crude morphological divisions between disks and spheroids in our sample, as well as details on the fitting techniques used are presented in Buitrago et al. (2008). Specifically, the Sérsic index and effective radii are obtained from fitting the following formula for the intensity of light at radii, r,

$$I_r = I_e \exp\left(-b_n\left[\left(\frac{r}{r_e}\right)^{1/n} - 1\right]\right), \quad (2)$$

where I_e is the intensity of light at the effective radii and n is the Sérsic index (with a value of $n = 4$ being equivalent to de Vaucouleurs' 1948 formula for an elliptical galaxy, and a value of $n = 1$ giving rise to an exponentially declining surface brightness profile appropriate for a disk-like object). r_e is the circularized effective radius, given by $r_e = a_e(1-\epsilon)^{1/2}$, where ϵ is the ellipticity and a_e is the semimajor axis of the best-fit ellipse to the galaxy light profile at the effective radius, r_e. b_n is a constant to be fit to the light profile.

The best-fit Sérsic profile is constructed via minimizing the residuals, which are defined as the difference between the *HST* F160W (H) band image and the model fit. We quantify the RFF (see Blakeslee et al. 2006 and Hoyos et al. 2012), which is a proxy for "badness of fit," as

$$\mathrm{RFF} = \frac{\left(\sum |\mathrm{Res}| - 0.8 \times \sigma_{\mathrm{image}}\right)}{\mathrm{FLUX}_{A_{2e}}}, \quad (3)$$

where the summation is performed over the total area within the ellipse fit of the galaxy within two effective radii, A_{2e}. |Res| is the absolute (modulus) value of the residual image and $\mathrm{FLUX}_{A_{2e}}$ is the total flux within the area of the ellipse within two effective radii for the observed image. σ_{image} is defined as

$$\sigma_{\mathrm{image}} = \left(\sigma_{\mathrm{Bkg}}^2 + \frac{F}{g}\right), \quad (4)$$

where g is the effective gain of the NIC-3 camera, F is the flux value from the model for each pixel, and σ_{Bkg} is the standard deviation of the background (noise) from the observed H band images.

The RFF statistic computes the fraction of light, present or absent in the residual image, which is not explained by empirical errors in the Sérsic model (for more details see Hoyos et al. 2012). This effectively equates to a measure of how reliable each fit is, with a lower number indicating a more reliable fit. Since this type of fitting assumes intrinsically symmetric light profiles of galaxies, it may be expected that it would not perform well on more asymmetric galaxies (or those with a high A value, as defined in Section 3.1). To investigate the possibility of a correlation here between poorness of GALFIT fitting (RFF) and asymmetry (A) in high-mass high-redshift galaxies, we plot these variables against each other in Figure 5.

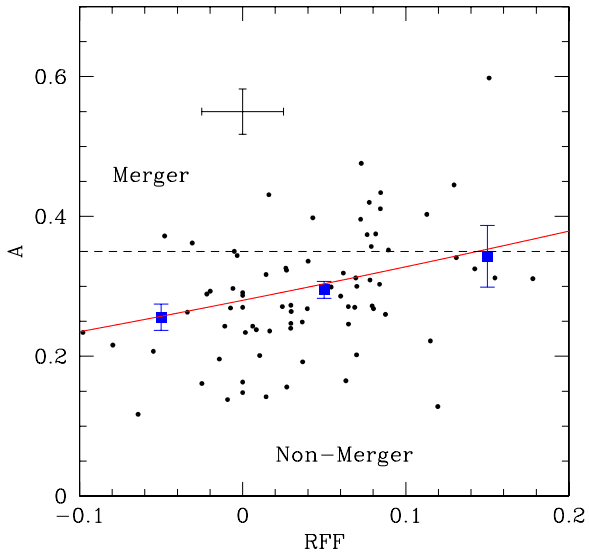

Figure 5. Asymmetry (A) vs. residual flux fraction (RFF) from GALFIT Sérsic index fitting for our sample of massive ($M_* > 10^{11}\ M_\odot$) galaxies at $z = 1.7$–3. The black dots are the unbinned data, with the black error bar representing average 1σ errors on RFF and A. The blue squares represent mean values of A, in the RRF ranges −0.1–0, 0–0.1, and 0.1–0.2, with their corresponding error bars being 2σ errors on the mean in each case. The solid red line is a best-fit simple power law to the unbinned data, which is defined in Section 3.1.3.

(A color version of this figure is available in the online journal.)

We find that there is a correlation between RFF and A, whereby galaxies with higher asymmetries tend to have worse fits from the GALFIT analysis. In fact we find that the mean value of A rises with 3σ significance from low to high RFF values, taking the errors as standard error on the mean and incorporating into this the intrinsic errors from the RFF and A methods. A best-fit, least-squares, simple power law to the unbinned data is found to be

$$A = (0.28 \pm 0.13) \times (1 + \mathrm{RFF})^{1.6\pm0.7}. \quad (5)$$

This implies that asymmetry in the light profile of massive galaxies at high redshifts may be a significant impediment to the use of Sérsic profile fitting for some systems. In these cases a non-parametric fit (such as *CAS*) will be more representative, since it makes no underlying assumptions about the spatial symmetry of the galaxy light profile. Furthermore, this relation opens the possibility to potentially identify likely candidates for mergers via high RFF values. For example, we find that galaxies with RFF > 0.05 are $\sim$4 times more likely to be mergers (as defined by *CAS*, see Section 3.1.2) than those with RFF < 0.05. From a K-S test this represents a 3σ significant rise from low to high bins of RFF in A. A high degree of scatter remains around the line of best fit. This is most probably explained by the errors inherent in measuring *CAS* and the RFF, as very few galaxies lie further than 2σ from the best-fit line. However, a much larger sample of galaxies with more general properties is needed to really establish this result. Nonetheless, our results are consistent with Sérsic methods being successful for spheroids and disks, but failing with irregular galaxies, i.e., the dominant cause of poor GALFIT profile fitting is morphological disturbance

for high-mass high-redshift systems. These results are also consistent with one of the overarching conclusions of this paper, i.e., that a significant fraction of high-redshift massive galaxies are highly disturbed, most likely by major merging, with ∼30% of systems giving rise to a poor Sérsic fit (RFF > 0.05) and ∼10% leading to a very poor fit (RFF > 0.1). This provides additional evidence that our samples of high-z massive galaxies are highly morphologically irregular to the non-parametric *CAS* approach (outlined in the preceding sections): they are frequently not fit well by parametric approaches.

3.2. Total Merger Fraction from Pair Statistics

3.2.1. Basic Method

Most probes of the merger histories of massive galaxies are considerably limited by constraints due to the depth of the imaging used. This is especially the case at higher redshifts. For this reason the vast majority of merger histories in the literature (at least all those which extend beyond $z > 1$) are restricted to "major" mergers. Although this definition varies from paper to paper, it is common to use a difference such as ±1.5 mag (>1:4 by stellar mass) for close pairs, as in Bluck et al. (2009), which corresponds to a similar mass range for which *CAS* is most sensitive (see also Conselice et al. 2009 for a discussion of this). Some recent studies have probed deeper into the minor merger regime (e.g., Hopkins et al. 2010; Lopez-Sanjuan et al. 2011; Lotz et al. 2011) but these usually only go down to a stellar mass ratio of 1:10 or less, and concentrate at lower redshifts than this study ($z < 1.5$).

Due to the exceptionally deep *HST*/NICMOS imaging we have acquired in the GNS, we are in a position to go much deeper, down to +3.5 mag at $z = 3$ and +4.8 mag at $z = 2.3$. This allows us to probe a mass range of up to a factor of ∼100 according to our photometric estimates, looking specifically at galaxies with masses $M_* = 10^9\ M_\odot$–$10^{11.5}\ M_\odot$ around massive galaxies with $M_* > 10^{11}\ M_\odot$. Thus, we can probe the total merger history of the most massive galaxies in the universe down to a threshold sensitivity of $M_* \sim 10^{9-9.5}\ M_\odot$, all the way back to $z = 2$–3. This considerably expands upon all previous attempts to ascertain the merger history of massive galaxies by increasing the threshold sensitivity by over a factor of 10 for high-redshift galaxies.

We define the total merger fraction, f_m (in analogy to the major merger fraction of Bluck et al. 2009), to be

$$f_m = \frac{1}{N}\sum_{i=1}^{i=N}(\mathrm{counts_i} - \mathrm{corr_i}), \tag{6}$$

where

$$\mathrm{corr} = \int_{m-1.5}^{m+m^+} \rho \times \pi\left(r^2_{30\,\mathrm{kpc}} - r^2_{5\,\mathrm{kpc}}\right)dm', \tag{7}$$

N is the total number of massive galaxies in the sample at each redshift range, and counts_i is the number of galaxies within the magnitude range $m-1.5$ to $m+m^+$ contained within the annulus of 5–30 kpc ($h = 0.7$) around each massive host galaxy. We use $m-1.5$ as the lower limit to our integral to assure that we count virtually all mergers down to the upper limit $m+m^+$. There are very few, if any, galaxies which are greater than 1.5 mag brighter than the massive galaxies we probe at high redshifts, given that there are extremely few galaxies with $M_* > 10^{11.5}\ M_\odot$ at $z > 1.7$.

The value corr is the background correction, which we compute from the surface number density, ρ, of galaxies within the magnitude range under consideration, from our GNS survey. The fact that we take our surface number densities from the same survey (around the objects being studied at radii < 200 kpc), which is centered around massive galaxies at high redshifts, reduces the risk of our results being unduly affected by differential redshift projection effects due to the increased clustering of massive galaxies at high redshifts (Bluck et al. 2009). This surface number density is then converted to an expectation value for the total number of close pairs one would measure by line of sight contamination via multiplying over the area of sky contained within the annulus of 5–30 kpc around each massive host galaxy. We adopt this annulus method, as opposed to a simple circle approach, to avoid effects from the contamination of the light profiles of the merging galaxies by the host galaxy's brightness. Since these massive galaxies are extremely compact (see Buitrago et al. 2008) we find an inner radii of 5 kpc to be more than sufficient to remove this effect.

Typical contamination corrections vary according to the stellar mass ratio of the pairs and the precise magnitudes of the galaxies in question. The major close pairs are corrected by typically up to a factor of two or so, with the more minor close pairs reduced by more than this, up to a factor of three to four. This is intuitive because the broader the magnitude range used, hence the larger the mass ratio examined, the more contaminants from foreground and background galaxies arise in the sample. Furthermore, to convert from a pair fraction to a merger fraction requires the use of a merger timescale. These are found to be in general longer for larger differences in the mass of two merging galaxies (see Lotz et al. 2008a, 2008b, 2010 where this is determined through detailed N-body simulation), i.e., minor mergers take longer than major mergers if all other factors, including the host, are the same. The exact form of the merger timescale dependence on mass ratio is unknown, however, but may lead to up to a factor-of-five difference in time from 1:4 major mergers to 1:100 minor mergers. All of this leads to the frequency of minor merging being suppressed when compared to major merging, and not proportional to the galaxy stellar mass function, as one may naively expect.

3.2.2. Method Test—The Millennium Simulation

The aim of this subsection is to compare the merger fraction results obtained by the statistical close pair methods presented in this paper (and in Bluck et al. 2009) with spectroscopic close pair methods for a set of model galaxy catalogs constructed from the Millennium Simulation. In particular, we use light cone views developed by Kitzbichler & White (2006) constructed from semianalytic galaxy catalogs in the Millennium Simulation produced by De Lucia & Blaizot (2007). The techniques used, and full details of the models, are provided in these references. For the purposes of this section it should suffice to comment that the views were a set of six pencil beam light cone observations through an extended Millennium Simulation, whereby 500 h^{-3} Mpc^3 blocks were added together with a small angular shift to avoid exact repetition. The full prescriptions for assigning galaxy luminosities and masses from halo masses are beyond the scope of this paper, but are presented (for the interested reader) in detail in De Lucia & Blaizot (2007) and references therein. Effectively, the catalogs from De Lucia & Blaizot (2007) provide the fundamental characteristics of the galaxies, such as stellar mass, luminosity, and location in the model coordinates system, and the tables from Kitzbichler & White

Table 2
Close Pair Method Test: Model Spectroscopy from the Millennium Simulation

Run ID	$N_{\rm hosts}$	$N_{\rm total}$	f_m (Stats)	f_m ($<500\,{\rm km\,s^{-1}}$)	f_m ($<1000\,{\rm km\,s^{-1}}$)	f_m ($<1500\,{\rm km\,s^{-1}}$)
1	44	30738	0.149 ± 0.022	0.068 ± 0.010	0.114 ± 0.017	0.159 ± 0.024
2	43	31295	0.247 ± 0.038	0.210 ± 0.032	0.233 ± 0.036	0.280 ± 0.043
3	82	31921	0.110 ± 0.012	0.061 ± 0.007	0.098 ± 0.010	0.146 ± 0.016
4	49	32501	0.161 ± 0.023	0.121 ± 0.017	0.167 ± 0.024	0.198 ± 0.028
5	62	33770	0.152 ± 0.019	0.097 ± 0.012	0.113 ± 0.014	0.168 ± 0.021
6	84	31948	0.189 ± 0.020	0.123 ± 0.013	0.166 ± 0.018	0.221 ± 0.024
7	54	34376	0.161 ± 0.022	0.019 ± 0.003	0.093 ± 0.013	0.167 ± 0.023
8	65	31727	0.191 ± 0.024	0.070 ± 0.009	0.142 ± 0.018	0.161 ± 0.020
Mean	60	32285	0.170 ± 0.040	0.095 ± 0.050	0.142 ± 0.045	0.188 ± 0.044

Notes. This table presents the results from a series of eight Millennium Simulation run tests on the efficacy of the close pair method presented in this paper and Bluck et al. (2009). Presented here are close pair fractions deduced statistically and through a spectroscopic-like method for comparison. The final row presents the mean properties across the varying tests. The models used were taken from the Kitzbichler & White (2006) view of the De Lucia & Blaizot (2007) semianalytic galaxy catalog for the Millennium Simulation. Please see http://www.g-vo.org/Millennium for full details and to access the mock catalogs used here for further investigation. The errors on individually calculated merger fractions are simple Poisson counting errors, with the errors presented for the mean values being the standard deviation about the mean across the eight runs performed.

(2006) provide the direct observational components, such as R.A. and decl., observed (spectroscopic) redshifts, and apparent K-band magnitudes.

We selected eight areas of the Kitzbichler & White (2006) views, with equal (0.01 deg^2) areas which provide our eight unique runs. This was chosen to contain roughly equal high-redshift massive galaxy numbers as our GNS sample, and to keep to a minimum the computational overheads that go with very large numbers of total galaxies visible in the view. The average number of $M_* > 10^{10.5}\,M_\odot$ galaxies at $1.7 < z < 3$ in each run is 60 (comparable to the 80 used in the GNS sample). The average number of galaxies visible at all redshifts and stellar masses in each view is ~32,000. This provides ample numbers to gain meaningful statistics on the differences between spectroscopic and statistically deduced close pair fractions from model data. We were forced to choose slightly lower stellar mass cuts than used in the GNS ($\log[M_*] > 11$) due to the intrinsic underpopulation of very massive galaxies (and halos) at high redshifts inherent in the Millennium Simulation (see, e.g., Bertone & Conselice 2009 for a discussion on this issue). However, the mass and redshift parameter space is broadly similar and should provide a good first formal test to the efficacy of the close pair method.

For each Millennium run we selected two samples: a high stellar mass, high-redshift galaxy catalog containing only $M_* > 10^{10.5}\,M_\odot$ galaxies at $1.7 < z < 3$, and a large catalog containing all galaxies viewed in the light cone and restricted area utilized, regardless of mass or redshift. We then ran our close pair codes (exactly as presented in Section 3.2.1 on our real data) and further ran an additional set of three spectroscopic close pair calculations (corresponding to massive galaxies with pairs within 30 kpc, with magnitudes ± 1.5 of the host galaxy magnitude, and velocity differences of $\Delta v < 500\,{\rm km\,s^{-1}}$, $1000\,{\rm km\,s^{-1}}$, and $1500\,{\rm km\,s^{-1}}$, respectively) utilizing the observed (spectroscopic) redshifts available for all objects in the view from the Kitzbichler & White (2006) catalogs. Explicitly, we compute the model spectroscopic pair fractions as

$$f_{\rm pair} = \frac{N_{\rm pair}(<30\,{\rm kpc}; \pm 1.5\,{\rm mag}; \Delta V < X)}{N_{\rm host}}, \qquad (8)$$

where $N_{\rm pair}$ gives the total number of galaxies in the model with companions within 30 kpc of the host, and within ± 1.5 of the host galaxy's K-band magnitude, with a velocity difference from the model-observed spectroscopic redshift of $X = 500\,{\rm km\,s^{-1}}$, $1000\,{\rm km\,s^{-1}}$, and $1500\,{\rm km\,s^{-1}}$. The statistical pair fraction is computed as in Equation (6) where the corrections for our statistical method are computed exactly as in Equation (7) in Section 3.2.1, with these corrections being taken around the objects in question (at radii < 200 kpc in physical units). The results are presented in Table 2.

Graphs showing and comparing the modeled spectroscopically and statistically deduced pair fractions are presented in Figure 6. We find that our statistical close pair method gives values which are in general lower than $\Delta v < 1500\,{\rm km\,s^{-1}}$ spectroscopic close pairs and higher than $\Delta v < 500\,{\rm km\,s^{-1}}$. We also note that in all but one case (run 4) our statistical methods are slightly higher in value than the $\Delta v < 1000\,{\rm km\,s^{-1}}$ spectroscopic close pairs. Quantitatively, we calculate a mean difference of $+0.075 \pm 0.04$ between statistical and spectroscopic close pairs (with $\Delta v < 500\,{\rm km\,s^{-1}}$); $+0.029 \pm 0.021$ between statistical and spectroscopic close pairs (with $\Delta v < 1000\,{\rm km\,s^{-1}}$); and -0.018 ± 0.23 between statistical and spectroscopic close pairs (with $\Delta v < 1500\,{\rm km\,s^{-1}}$). The errors presented here are taken as the standard deviation about the mean difference in values.

Care must be taken when utilizing these raw results to attempt to transform these into updated errors on the statistical method. Since the environmental data on our sample of high-redshift high stellar mass galaxies (presented in Grützbauch et al. 2011a, 2011b) place these objects as primarily in groups, as opposed to field or cluster galaxies, this would seem to suggest that velocity dispersions ought to be $\sim 300\,{\rm km\,s^{-1}}$. This is, unfortunately, not ideal when using the Millennium Simulation as the smoothing length inherent to the halo merger trees results in there being very few galaxies in close pairs with low ($\Delta v < 500\,{\rm km\,s^{-1}}$) relative velocities for artificial reasons. As such, the exact velocities cannot be entirely trusted at small distances, which is the area of interest for this study. A full quantitative analysis of the effects of the smoothing length in the Millennium Simulation on overpopulating close pairs with higher velocities is beyond the scope of this paper. Nonetheless, it can be seen that the $\Delta v < 500\,{\rm km\,s^{-1}}$ spectroscopic close pairs scale less well with both the statistical method and the higher velocity difference spectroscopic methods, and we tentatively suggest that this is ultimately a result of the smoothing scale length in the Millennium Simulation.

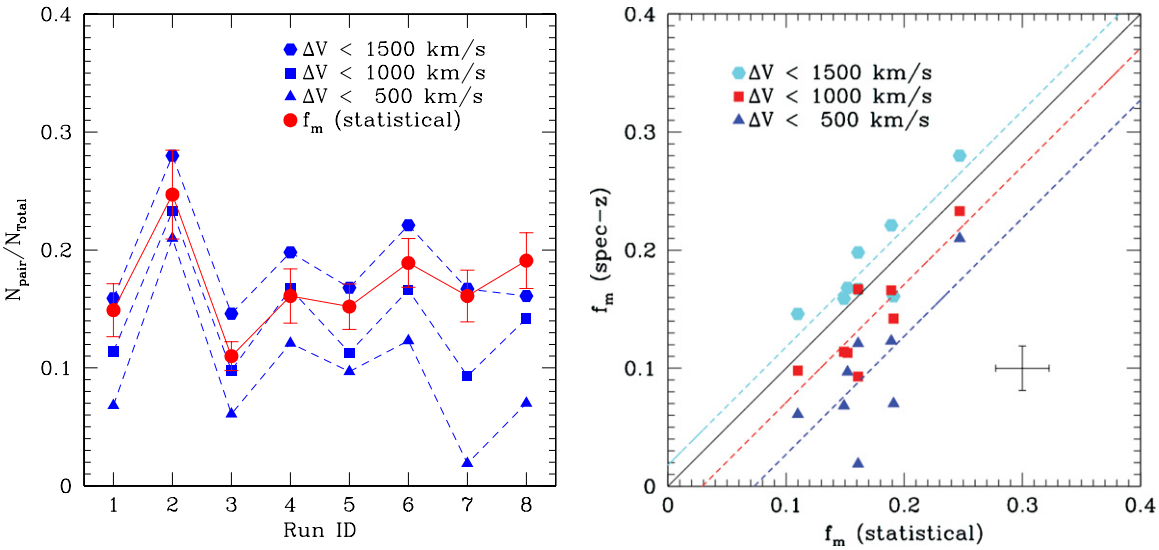

Figure 6. Left panel is a comparison of modeled spectroscopic and statistical pair fractions ($f_{\rm pair} = N_{\rm pair}/N_{\rm Total}$) across the eight runs performed on the Kitzbichler & White (2006) views of the De Lucia & Blaizot (2007) galaxy models drawn from the Millennium Simulation. The differently shaped blue points are for modeled spectroscopic pair fractions using varying velocity differences, as shown on the plot. The red squares are the modeled statistical pair fractions of each independent run, with the errors on these being Poisson counting errors. These are the values we would measure using our method. The right panel presents model spectroscopically confirmed close pairs at varying velocity differences as a function of the modeled statistically deduced pair fraction (which we use on actual galaxies later in this paper). The black error bar represents the average counting error on all methods. These errors do not take into account cosmic variance, systematic effects, or biases as this is in part what these plots aim to address. The solid black line indicates the one-to-one relation. The cyan, red, and blue dashed lines indicate best fits to the $\Delta v = 1500$, 1000, and 500 km s^{-1} modeled spectroscopic close pair fractions, respectively, assuming a constant one-to-one gradient and varying the intercept only. Explicitly, f_m (spec-z) $= f_m$ (statistical) $- c$, where $c = -0.018$ for 1500 km s^{-1}, +0.029 for 1000 km s^{-1}, and +0.071 for 500 km s^{-1}.

(A color version of this figure is available in the online journal.)

If we consider the $\Delta v < 1000$ km s^{-1} spectroscopic close pair as the real values for close pairs (which is often used in the literature to incorporate galaxies with relative velocities $\Delta V < 3\sigma_{\rm group}$), then we witness a relatively small offset of $+0.029 \pm 0.021$ from the modeled spectroscopic close pair fraction when compared to our statistical approach, which is smaller than the average statistical random errors for our high-redshift data (± 0.07). It is also interesting to note that this effect is comfortably within 2σ of indicating no intrinsic bias at all. What is established here is that there is broad agreement between spectroscopic and statistical close pair methods when applied to the model data of the Millennium Simulation. There is a hint of a small possible bias for the statistical method to overestimate the spectroscopic method at $\Delta v < 1000$ km s^{-1}, but this is only visible at the $<2\sigma$ level and contributes a significantly smaller shift than the random errors on our data at high redshifts. This implies that we can reliably use our close pair method at high redshifts for massive galaxies to an accuracy determined by the random errors.

3.2.3. Merger Timescales

Unfortunately, the mechanics of the Millennium Simulation's semianalytics makes it difficult to use for probing the merger timescales directly. There is neither sufficient resolution nor detailed enough gas physics implemented to trust the timescales between close pairs becoming mergers; thus, this is not explored further here. The most realistic models to date are implemented by Lotz et al. (2008a, 2008b, 2010). These are based on gas-rich disk mergers (Sbc models) and are computed via N-body simulations. The values they obtain are used toward the end of this paper, but it is acknowledged that uncertainty in the initial relative velocities remain an unrestricted source of error in these analyses at the present time.

Future planned spectroscopic study, as well as even more detailed and realistic N-body simulations, will come to improve the constraints on this difficult issue in time. For now, adopting average group velocity dispersions of typically $\sigma_{\rm group} \sim 300$ km s^{-1} and looking principally at gas-rich disks have yielded workable values of the merger timescale (τ_m). In light of the uncertainty in this issue, however, in the following sections the majority of the analyses are performed in a timescale-independent manner, and where possible timescales are factored out of the equations until the final values are stated to make it easy for researchers in the future to implement new timescales into our analyses, when these are better constrained than at present.

3.2.4. Total Merger History: Results and Fitting

In order to probe the total merger history of massive galaxies at high redshifts, we vary the upper limit to the magnitude range of interest (m^+ in Equation (7)) from 1.5 to 6.5 in increments of 1.5 (covering a mass ratio up to $M_*^{\rm host}/M_*^{\rm pair} \sim 100$), probing the total merger fraction. We also probe an ultra-major merger fraction (>1:2 by mass) of $m^+ = 0.5$. See Figure 7 for typical examples of major close pairs, and Figure 8 for typical examples of minor close pairs. The results of this are plotted in Figure 9. The vertical dotted lines indicate the completion limits for each redshift range probed from the GNS (see Conselice et al. 2011a for full details on deducing our mass and magnitude completion thresholds). Essentially, we compare our number counts of galaxies at differing magnitudes to those of the much deeper Hubble Deep Field (HDF), and conclude that our limits are where these curves cease to agree closely (data for the HDF-N comes from Thompson et al. 1999 and for the HDF-S from Metcalfe et al. 2006).

We witness a rise in merger fraction with magnitude range out to the completion limits. We note that the major and minor pair systems are in general different populations, with only ~20%

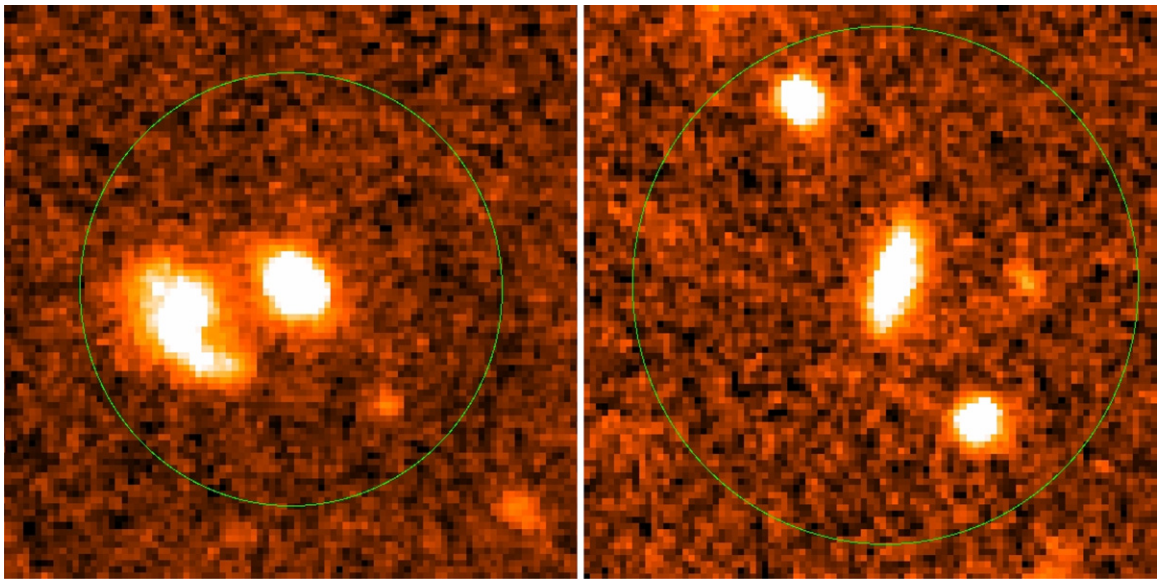

Figure 7. Typical examples of major close pairs: 1:4 < r_{M_*} < 4:1. *HST*/NICMOS H_{160} image of GNS-8214 (left) and GNS-373 (right). The green circle indicates the $d < 30$ kpc (in physical units) region we use to select close pairs within.
(A color version of this figure is available in the online journal.)

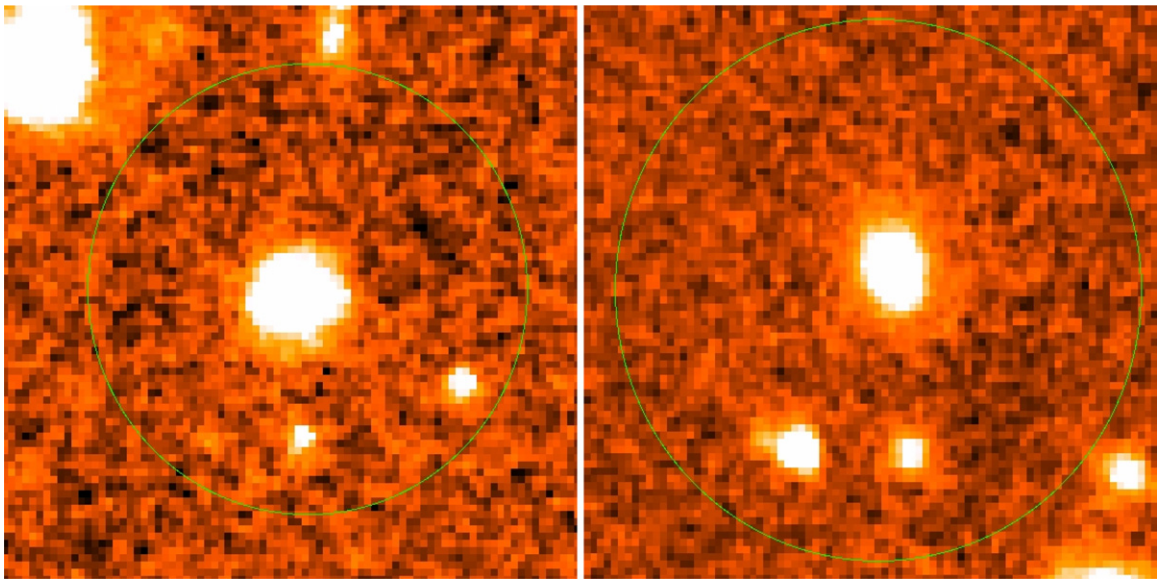

Figure 8. Typical examples of minor close pairs: 1:100 < r_{M_*} < 1:4. *HST*/NICMOS H_{160} image of GNS-7979 (left) and GNS-840 (right). The green circle indicates the $d < 30$ kpc (in physical units) region we use to select close pairs within.
(A color version of this figure is available in the online journal.)

of major mergers also being identified with minor merging. We also present a rough guide to the masses of objects included at the top of Figure 9. This is computed by assuming a mass-to-light ratio of 2.5:1 (i.e., $\Delta H_{\rm AB}/\Delta \log M_* = 2.5$) as frequently implemented in the literature, and a mean stellar mass for the host galaxies of $M_* \sim 10^{11}\,M_\odot$.

We fit the merger fraction dependence on magnitude range up to the respective completion limits (of + 3.5 mag at $z = 3$ and + 4.8 mag at $z = 2.3$). At $2.3 < z < 3$ we find that the merger fraction dependence on magnitude range is

$$f_m(\delta H_{\rm AB}) = (0.12 \pm 0.07) \times (1.5 + \delta H_{\rm AB})^{0.91\pm0.35}; \quad (9)$$

at $1.7 < z < 2.3$ we find a slightly steeper dependence of

$$f_m(\delta H_{\rm AB}) = (0.04 \pm 0.03) \times (1.5 + \delta H_{\rm AB})^{1.24\pm0.37}. \quad (10)$$

Assuming a mass-to-light ratio, the above equations may be converted to the merger fraction dependence on mass range (δm_*). We use a mass-to-light ratio of 2.5:1 (L : M), and define $\delta m_* = 11.5 - \log(M_*^{\rm pair}[M_\odot])$, where $M_*^{\rm pair}$ is the stellar mass of the paired galaxy, and $\log(M_*) = 11.5$ is chosen as the upper limit to a major merger, since there are extremely few, or no, galaxies with stellar masses greater than this at $z > 1.7$. Thus, at $2.3 < z < 3$ we find a merger fraction dependence on mass range for massive galaxies of

$$f_m(M_*) = (0.28 \pm 0.17) \times \delta m_*^{0.91\pm0.35}, \quad (11)$$

and at $1.7 < z < 2.3$ we find a merger fraction dependence on mass range for massive galaxies of

$$f_m(M_*) = (0.12 \pm 0.09) \times \delta m_*^{1.24\pm0.37}. \quad (12)$$

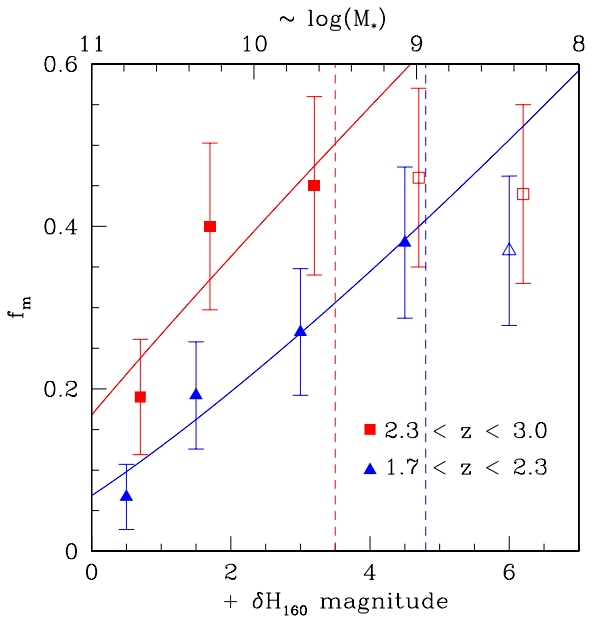

Figure 9. Merger fraction (f_m) as a function of magnitude range ($+\delta H_{160}$) and approximate stellar mass sensitivity threshold ($\sim\log(M_*)$) for massive galaxies (with $M_* > 10^{11}\,M_\odot$). The data points are separated into two redshift ranges as displayed on the plot. The error bars displayed are 1σ Poisson errors on the statistical counting. The vertical dotted lines indicate the completeness limits for each redshift range, respectively. Solid symbols indicate merger fractions computed where we are complete, and open symbols indicate merger fractions computed where we are incomplete. The solid lines are best-fit simple power-law functions to the merger fraction dependence on mass/magnitude range for each redshift range (see Section 3.2.4 for further details).

(A color version of this figure is available in the online journal.)

This gives a prescription for deducing the probable total (minor + major) number of mergers from extrapolation of these trends via the following methodology.

The total number of mergers, within a given mass and redshift range, is given by calculating the double integral:

$$N_m = \int_{t_1}^{t_2} \frac{1}{\Gamma(z, M_*)}\, dt = \int_{t_1}^{t_2}\int_{M_1}^{M_2} \left[\frac{1}{\Gamma(z, M_*)}\right]' dM_*\, dt \tag{13}$$

$$= \int_{z_1}^{z_2} \frac{t_H}{(1+z)E(z)} \int_{M_1}^{M_2} \left[\frac{1}{\Gamma(z, M_*)}\right]' dM_*\, dz, \tag{14}$$

where

$$\left[\frac{1}{\Gamma(z, M_*)}\right]' = \frac{d}{dM_*}\left(\frac{f_{gm}(z, M_*)}{\tau_m(M_*)}\right) \tag{15}$$

and

$$f_{gm}(z, M_*) = f_m(z, M_*)|_{\rm minor} \;\; \text{or} \;\; \sim \left.\frac{2 \times f_m(z, M_*)}{1 + f_m(z, M_*)}\right|_{\rm major}. \tag{16}$$

$\Gamma(z, M_*)$ is the characteristic time between mergers, t_H is the Hubble time, $f_m(z, M_*)$ is the merger fraction, $f_{gm}(z)$ is the galaxy merger fraction (i.e., the number of galaxies merging, not the total number of mergers), $\tau_m(M_*)$ is the merger timescale (which we assume to be redshift invariant), and the parameter $E(z) = [\Omega_M(1+z)^3 + \Omega_k(1+z)^2 + \Omega_\Lambda]^{1/2} = H^{-1}(z)$, which we evaluate for a flat spacetime with a ΛCDM cosmology as defined in Section 1.

We construct a parameterization of the total galaxy merger fraction dependence on redshift, derived at our mass completion threshold of $\log(M_*) \sim 9$; thus

$$f_{gm}(z)|_{M_*>10^9\,M_\odot} = f_{gm}(z=0)|_{M_*>10^9\,M_\odot} \times (1+z)^\alpha. \tag{17}$$

Since we have only two independent redshift values for the total galaxy merger fraction derived at our completion limit, we are not able to constrain the form of this function particularly well at present. As such, to model our errors, we allow the exponent, α, to vary from 0.5 to 5 and compute least-squares best fits to $f_{gm}(z=0)$, taking into account the errors on our initial data points. We find that $f_{gm}(z=0)$ varies from 0.40 at $\alpha = 0.5$ to 0.001 at $\alpha = 5$. This range in α is wide enough to incorporate almost all measured values of the merger fraction dependence on redshift for major and minor mergers computed to date (e.g., Patton et al. 2000; Rawat et al. 2008; Conselice et al. 2008, 2009; Bluck et al. 2009; Lopez-Sanjuan et al. 2010a, 2010b; Hopkins et al. 2010). We then use this variance as an estimator to compute our underlying error in measuring the total number of mergers.

To evaluate the total number of mergers a massive galaxy will experience in a given redshift interval we must simplify Equations (13) and (14), and apply these to our mass range of interest. Explicitly, we calculate the total number of mergers through this summation, an approximate numerical solution to the integration in Equation (14), evaluated for our mass range of interest:

$$N_m \approx \frac{1}{\langle\tau_m(M_*)\rangle} \sum_{z=z_1}^{z=z_2} \left(\frac{t_H}{(1+z)E(z)}\;\; f_{gm}(z)|_{M_*>10^9\,M_\odot}\right) \delta z, \tag{18}$$

where

$$\langle\tau_m(M_*)\rangle = \frac{\int_{M_1}^{M_2} \tau_m(M_*)\; dM_*}{\int_{M_1}^{M_2}\; dM_*}, \tag{19}$$

$M_1 = 10^9\,M_\odot$, and $M_2 = 10^{11.5}\,M_\odot$ for our study. All other variables are as defined above for Equations (13)–(17). Unfortunately, since the form of the function $\tau_m(M_*)$ is currently not well constrained we cannot compute the mean merger timescale directly here, but we include the general form for completion.

Evaluating this summation from $z_1 = 3$ to $z_2 = 1.7$ (the area probed directly in this study), we find that an average massive ($M_* > 10^{11}\,M_\odot$) galaxy will experience on average $N_m = (1.1 \pm 0.2)/\langle\tau_m(M_*)\rangle$[Gyr]) mergers with galaxies with $M_* > 10^9\,M_\odot$ over the redshift range $z = 1.7$–3. We estimate a total of $N_m = (4.5 \pm 2.9)/\langle\tau_m(M_*)\rangle$[Gyr] mergers with $M_* > 10^9\,M_\odot$ galaxies from $z = 3$ to the present via extrapolation of the trend. Note that the errors are considerably larger here due to our ignorance of the exponent of the redshift dependence of the galaxy merger fraction (f_{gm}), and hence the characteristic time between mergers (Γ) used in the integral computing the total merger number, N_m. We factor the merger timescale $\tau_m(M_*)$ out of our calculations (assuming that it is redshift independent) as this is poorly known for the mass range of galaxies probed in this paper. However, as a rough guide, Lotz et al. (2008a, 2008b, 2010) suggest that this might be ~0.4 Gyr for 3:1 mass mergers, and ~1 Gyr for 9:1 mass mergers from *N*-body simulations. This appears to be roughly a logarithmic dependence of timescale on stellar mass, suggesting that at 1:100 $\tau_m \sim 2$–3 Gyr, but this is currently unconstrained directly either by *N*-body simulations or observational approaches.

In order to calculate the stellar mass increase due to these major and minor mergers, we must compute an average mass

increase per merger. This is computed via the weighted mean from fits to the merger fraction dependence on mass range (see Figure 9 and Equations (11) and (12)). Specifically, we compute

$$\frac{\langle \Delta M_* \rangle}{N_m} = \int_{z_1}^{z_2} \left(\frac{\int_{M_1}^{M_2} M_* f'_{gm}(z, M_*) dM_*}{\int_{M_1}^{M_2} f'_{gm}(z, M_*) dM_*} \right) \frac{dz}{z}, \quad (20)$$

where we integrate over our mass range of interest from $10^9$to$10^{11.5}$ $M_\odot$. We note that the form of the function f_{gm}, i.e., its exponent, does not vary strongly with redshift between $z = 1.7$ and 3 (the range we probe directly). So, we take its average value and compute the errors from the extremes allowed by the fits. If, however, this is found to vary strongly with redshift from $z = 1.7$ to the present, our extended results will need to be recomputed accordingly in the future when deeper and wider low-redshift data are available.

We find $\langle \Delta M_* \rangle / N_m = (7.5 \pm 2.6) \times 10^{10}\ M_\odot$. In the redshift range probed directly by the GNS ($z = 1.7$–3), this corresponds to an average massive galaxy experiencing a mass increase of $\langle \Delta M_* \rangle = (8.3 \pm 3.2)/\langle \tau_m(M_*) \rangle$[Gyr] $\times\ 10^{10}\ M_\odot$. This leads to a total stellar mass increase over the past ∼12 Gyr ($z = 3$–0) from extrapolation, due to $M_* > 10^9\ M_\odot$ mergers, with massive ($M_* > 10^{11}\ M_\odot$) galaxies, of $\langle \Delta M_* \rangle = (3.4 \pm 2.2)/\langle \tau_m(M_*) \rangle$[Gyr] $\times\ 10^{11}\ M_\odot$.

A good first-order approximation to the actual value of $\tau_m(M_*)$ will be to take its value at our median mass of merger of $\sim 2 \times 10^{10}\ M_\odot$, i.e., ∼1 Gyr, from *N*-body simulations in Lotz et al. (2010). When compared to the major merger stellar mass increase, computed in Bluck et al. (2009), of $(1.7 \pm 0.5) \times 10^{11}\ M_\odot$, this suggests that minor mergers contribute a similar amount of stellar mass to major mergers from $z = 3$ to the present, with a minor merger stellar mass increase of $\sim 1.7 \times 10^{11}\ M_\odot$. It is still, however, possible that ultra-minor mergers of massive galaxies with $M_* < 10^9\ M_\odot$ galaxies will be so numerous that they will significantly affect the mass increase of massive galaxies, although this seems very unlikely given the trends and analyses presented in this paper, and the longer timescales they will experience due to larger differences in mass ratio.

The average stellar mass of our GNS massive galaxy sample is $\langle M_* \rangle = 1.7 \times 10^{11} M$. Thus, the mass increase due to all mergers down to a stellar mass sensitivity threshold of 1:100 over the redshift range probed directly by this study ($z = 3$ to $z = 1.7$) is $\delta M_*/M_* = 0.49 \pm 0.21$, with ∼65% of this increase coming from major mergers and ∼35% being due to minor mergers. Further extrapolation of this trend to $z = 0$ suggests that there may be a total mass increase $\delta M_*/M_* = 2.0 \pm 1.2$ per galaxy, with roughly equal contribution from major and minor mergers over this total period. This indicates a factor-of-three growth in mass, i.e., $M_*^{\rm final} = (1 + \delta M_*/M_*^{\rm initial}) M_*^{\rm initial} = 3 \times M_*^{\rm initial}$. But this value should be taken with more caution as we are unable to probe directly the evolution from $z = 1.7$ to the present. However, this value is consistent with other recent work on the minor merger histories of massive galaxies at lower redshifts in Lopez-Sanjuan et al. (2011) where they find a $\delta M_*/M_* \sim 0.4$ down to a stellar mass ratio of 1:10 from $z = 1$ to the present, using a maximum likelihood close pair method. In the same stellar mass and redshift regime, we find $\delta M_*/M_* \sim 0.3 \pm 0.25$ (note that our errors are large due to not probing this range directly in our study). Nonetheless, this demonstrates a consistency and possible complementarity between the approaches used here and in the work of Lopez-Sanjuan et al. (2011).

4. DISCUSSION

4.1. Mergers

In this paper, we have utilized several different methods to probe the structures and evolution of massive galaxies over cosmic time. First, it is important to acknowledge that there are extremely massive galaxies at $z > 2$, but their properties are somewhat different to local massive galaxies (see, e.g., Mortlock et al. 2011 for a study of the mass function at these redshifts). The most prominent difference is that these massive galaxies tend to have smaller effective radii for their masses (e.g., Buitrago et al. 2008). We find that ∼1/4 of all massive galaxies (with $M_* > 10^{11}\ M_\odot$) are highly morphologically disturbed at $1.7 < z < 3$, and in fact fit the rest-frame optical definition for a *CAS*-selected merger (see Section 3.1). This implies that major merging is an important factor in the evolution of massive galaxies, and qualitatively supports a hierarchical approach to galaxy formation. Moreover, we find close accord between ($d < 30$ kpc) close pair fractions and *CAS* merger fractions at all redshifts, up to $z = 3$ (see Figure 3). This strongly suggests that both approaches trace the underlying major merger activity in massive galaxies, and, furthermore, implies that the timescales involved in each approach must be similar (see Conselice et al. 2009 for a discussion of this effect at lower redshifts).

By way of comparison to other techniques, the stellar mass increase we compute from the total merger history down to a stellar mass threshold of $M_* > 10^9\ M_\odot$ agrees favorably with studies of the evolution of the mass function of massive galaxies from $z = 3$ to the present, see, e.g., Mortlock et al. (2011). By examining the stellar mass function's evolution over cosmic time, one can place an approximate upper limit to the mass increase massive ($M_* > 10^{11}\ M_\odot$) galaxies can undergo from $z = 3$ to the present, of less than a factor of eight. This value, however, has large errors of approximately a factor of two or so on the upper limit. Further analysis of star formation in these massive galaxies (performed in Bauer et al. 2011) lends an additional factor-of-two or so stellar mass increase via star formation. Therefore, by merging and star formation we could expect our massive galaxies to increase in mass by around a factor of four to six, consistent with the less than a factor-of-eight prediction from analysis of the stellar mass function evolution. Ultimately, this suggests that both merging (major and minor) and star formation are important in the stellar mass buildup of massive galaxies over the past 12 Gyr. The final piece to this puzzle is cool gas accretion onto galaxies, which will be considered in a forthcoming paper in this GNS series (C. J. Conselice et al. 2012, in preparation).

4.2. Size Evolution

Numerous studies over the past five years have found increasingly compelling evidence for dramatic size evolution of massive galaxies over the past ten or so billion years (e.g., Daddi et al. 2005; Trujillo et al. 2006, 2007; Buitrago et al. 2008; Cimatti et al. 2008; van Dokkum et al. 2008, 2009; Carrasco et al. 2010). It is currently widely argued that massive galaxies may grow in size by up to a factor of five since $z = 3$, largely due to stellar mass buildup in the outer regions (or wings) of these galaxies. While there are still concerns that some of this apparent size evolution may be driven by Sérsic fitting of massive galaxies at high redshifts not being the best way to represent the luminosity profiles (e.g., Mancini et al. 2010), a wealth of evidence from simulation, and observational attempts to break the degeneracies inherent in former approaches, is coming to

establish the validity of this result (e.g., Cappellari et al. 2009; Onodera et al. 2010; Newman et al. 2010; van de Sande et al. 2011). If this size evolution is real, then it becomes of vital importance in contemporary astrophysics to address the question: *What drives the size increase of massive galaxies over cosmic time?*

Naab et al. (2009) and Khochfar & Silk (2006) have both argued from a theoretical standpoint for merger-driven size evolution of massive galaxies. We have, in this paper, estimated the total merger history of massive galaxies with $M_* > 10^9\,M_\odot$ galaxies (see Section 3.2.4). We found that there are ∼4.5 mergers predicted from $z = 3$ to the present, which may go some way toward explaining the observed size evolution of massive galaxies. In fact, arguments presented in Naab et al. (2009) suggest that a mass increase due to minor and major mergers of a factor of two could lead to size evolution of up to a factor four in radii. The more mergers there are the greater the size evolution, and thus a mass increase of a given magnitude will be more effective at increasing the size of the resultant galaxy if it is imparted in a series of minor mergers rather than one major merger. Thus, it is the relatively high fraction of mass imparted by minor mergers which is most useful for increasing a massive galaxy's size.

This can be seen quantitatively by assuming a virialized merging system, such that the final merged galaxy is virialized, and the two merging galaxies are also virialized. This is a realistic and theoretically motivated scenario as Khochfar & Burkert (2006) show that dark matter halos merge predominantly on parabolic orbits, thus conserving energy, within current leading cosmological simulation. Thus, from the virial formula, $2K + W = 0$, we have (as in Naab et al. 2009; Binny & Tremaine 2008)

$$E_i = K_i + W_i = -K_i = \frac{1}{2}W_i \tag{21}$$

$$= -\frac{1}{2}M\langle v_i^2\rangle = -\frac{1}{2}\frac{GM_i^2}{r_{g,i}}, \tag{22}$$

where E_i is the total energy, M_i is the total mass, $\langle v_i^2\rangle$ is the mean square velocity, and $r_{g,i}$ is the gravitational radius of the initial host massive galaxy (i.e., the radius at which mass M_i is contained). By defining the total energy of the (major or minor) merging galaxy (as in Naab et al. 2009) as E_a, and the total energy of the final resultant merged galaxy as E_f, with all other variables similarly labeled (e.g., M_a is the mass of the major or minor merging galaxy etc.), we have, assuming a fully virialized system,

$$E_f = -\frac{1}{2}\frac{GM_f^2}{r_{g,f}} = E_i + E_a = -\frac{1}{2}\frac{GM_i^2}{r_{g,i}} - \frac{1}{2}\frac{GM_a^2}{r_{g,a}} \tag{23}$$

$$= -\frac{1}{2}\frac{(1+\eta\epsilon)GM_i^2}{r_{g,i}} = -\frac{1}{2}\frac{(1+\eta)^2GM_i^2}{r_{g,f}}. \tag{24}$$

Therefore,

$$\frac{r_{g,f}}{r_{g,i}} = \frac{(1+\eta)^2}{(1+\eta\epsilon)}, \tag{25}$$

where

$$\eta = M_a/M_i \quad \text{and} \quad \epsilon = \langle v_a^2\rangle/\langle v_i^2\rangle. \tag{26}$$

See Naab et al. (2009) for the original (slightly different) derivation and a detailed discussion.

The result of this is that minor mergers are a more efficient driver of galaxy growth than major mergers. This is because, for a similar total mass increase, there will be a greater growth in size if this mass is imparted as a series of smaller mergers rather than one big merger due to the smaller value of ϵ in this case. Further details on these arguments as well as detailed derivations can be found in Naab et al. (2009), Hopkins et al. (2009), and Bezanson et al. (2009).

For the mass increase due to minor mergers witnessed in this paper, of roughly a factor of two from $z = 3$ to the present, corresponding to $\eta_{\rm minor} \sim 1$ and $\epsilon_{\rm minor} \ll 1$, there should be a size increase of up to a factor of four. Furthermore, the mass increase due to major merging of another factor of the order of two by mass, corresponding to $\eta_{\rm major} \sim 1$ and $\epsilon_{\rm major} \sim 1$, would lead to a growth in size of up to a further factor of two. These estimates should be taken to be upper limits as it is probable that energy will be lost to the intergalactic medium during merging via a number of processes, including the formation of new stars, heating of interstellar gas, and igniting of AGN. Therefore, we can place an upper limit on the amount of massive galaxy growth allowable via major and minor merging from $z = 3$ to the present of a factor of <6. This is comparable to the observed factor of ∼4–5 growth in effective radii (seen in, e.g., Buitrago et al. 2008), suggesting that merging can be primarily responsible, with minor merging being the more efficient route, but that there may need to be additional contributors as well since these are upper limits. See Figure 10 for the allowable mass and size evolution for massive galaxies from $z = 3$ to the present.

This result is broadly consistent with recent work of Trujillo et al. (2011) where the authors conclude that ∼8 minor (1:10) mergers are required, or else ∼3 major (1:3) mergers, to bring high-redshift compact massive galaxies to the appropriate local mass–radius relation. We find that ∼4–5 mergers (with a range of stellar mass ratios from 2:1 to 1:100) take a massive galaxy between 50% and 100% of the required distance to the local relation from its average $z = 2$–3 location.

Therefore, the minor and major merger history witnessed in this work may be large enough to explain most of the growth witnessed in massive galaxies across the past 12 billion years (e.g., Trujillo et al. 2007; Buitrago et al. 2008) according to recent theoretical estimation (Naab et al. 2009). It is, however, still worth considering other contributive factors, such as the effect of the enormous outpouring of energy from supermassive black holes in the nuclei of massive galaxies over this same period of cosmic history (see Fan et al. 2008 and Bluck et al. 2011). It may yet prove probable that it is a combination of star formation, passive evolution, major and minor merging, and AGN "puffing up" which causes the size evolution of massive galaxies. This work, however, implies that merging by itself could be responsible for most of the observed size evolution, assuming the validity of the arguments presented in Naab et al. (2009) and appropriate gas fractions (dictating the energy losses complicating the purely virialized merger model), which are yet to be empirically deduced.

5. SUMMARY AND CONCLUSIONS

In this paper we study in detail the structures, morphologies, and total merger history evolution of a population of 80 extremely massive ($M_* > 10^{11}\,M_\odot$) galaxies at very high redshifts ($1.7 < z < 3$). We find that massive galaxies at high redshifts are frequently morphologically disturbed, with ∼1/4 meeting the criteria for a *CAS*-selected major merger (see Section 3.1.1). Furthermore, we note that close pair methods

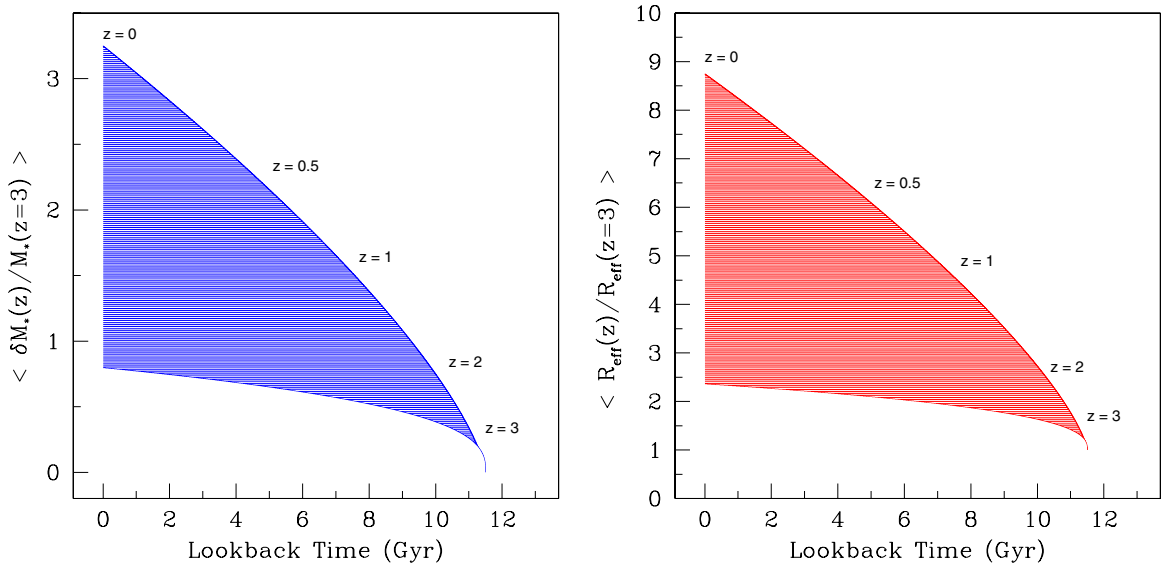

Figure 10. Left panel: permitted stellar mass evolution. Right panel: permitted size evolution. The stellar mass and size evolution are plotted as a function of look-back time, overlaid are the redshifts at these times. Both plots are normalized by the initial $z = 3$ value, so the uncertainty increases toward the present. Only the look-back times 8–11.5 Gyr are probed directly by this study, with a wide range of probable functions used to extrapolate to the present (see Section 3.2.4), which is responsible for the flaring of these plots out to $z = 0$. The size evolution (right) is computed as the maximum allowable for the stellar mass growth (left). See Section 4.2 for full details.

(A color version of this figure is available in the online journal.)

(with $d < 30$ kpc) to deduce major mergers find close accord with morphological *CAS*-determined major mergers at all redshifts, up to $z = 3$, indicative of both approaches being sensitive to the underlying merger history, and, moreover, having similar mass ratio and timescale sensitivities.

We find that the "poorness" of GALFIT fitting (RFF) is positively correlated with the global asymmetry of the galaxy (A) for high-redshift massive galaxies, see Section 3.1.3. Moreover, we find that galaxies with GALFIT fits defined as "poor" (RFF > 0.05) are over four times more likely to be highly asymmetric systems (with $A > 0.35$) than those galaxies with "good" (RFF < 0.05) fits, which suggests that Sérsic index fitting can be used to select likely major merger candidates through analysis of the RFF.

We also investigate the minor merger properties of our sample of massive galaxies down to a mass sensitivity threshold of $M_* = 10^9\ M_\odot$. In order to achieve this we utilize extremely deep and high-resolution H-band imaging from the *HST* GNS, which corresponds to rest-frame optical wavelengths at the redshifts probed in this paper ($z = 1.7$–3). We deduce that there are in total $N_m = (4.5 \pm 2.9)/\tau_m$ mergers from $z = 3$ to the present, which leads to massive galaxies growing in mass by a factor of $\sim$3 due to all mergers, with half of this mass increase being driven by minor mergers with galaxies of mass $M_* = 10^9$–$10^{10.5}\ M_\odot$. We go on to suggest that the size increase over cosmic time of massive galaxies could be driven by these mergers, noting that the number of mergers we compute for massive galaxies (and their resultant approximate threefold mass increase) could correspond to a size increase of up to a factor of six via the Naab et al. (2009) model. This is examined in detail in Section 4.2.

In conclusion, we find that massive galaxies are more asymmetric at high redshifts, have many more minor and major mergers at early times than late times, and grow in mass threefold from $z = 3$ to the present due to merging alone. We also suggest that the size evolution of massive galaxies must be partly (or possibly entirely) driven via this galaxy merging.

We thank Robert Chuter, Alfonso Aragon-Salamanca, Frazer Pearce, and Nina Hatch for insightful discussions and helpful suggestions on this work. We thank Emma Bradshaw for computational assistance with processing numerical solutions to complex integrals. We appreciate helpful suggestions and comments from the referee Andrew W. Zirm. We also gratefully acknowledge funding from the STFC and the Leverhulme Trust to carry out this research.

This work was supported by the Gemini Observatory, which is operated by the Association of Universities for Research in Astronomy, Inc., on behalf of the international Gemini partnership of Argentina, Australia, Brazil, Canada, Chile, the United Kingdom, and the United States of America.

APPENDIX

DATA TABLES

In Table 1, we present data on the fundamental properties, close pair statistics, and structures of the 80 massive ($M_* > 10^{11}\ M_\odot$) galaxies found within the GNS. $N_{\rm MP,corr}$ is the statistically corrected major pair fraction of each galaxy, with $N_{\rm TP,corr}$ the statistically corrected total pair fraction of each galaxy with paired galaxies with $M_* > 10^9\ M_\odot$. A is the asymmetry of the massive galaxy, with C being its concentration. Typical errors are $\langle A_{\rm err}\rangle = \pm 0.05$, $\langle C_{\rm err}\rangle = \pm 0.26$, and $\sim$0.3 dex for stellar mass.

Full data catalogs are available at http://www.nottingham.ac.uk/~ppzgns/index.html, where all computed values and initial error estimations are publicly available. Please see Conselice et al. (2011a) for a companion to these data products.

REFERENCES

Bauer, A., Conselice, C. J., Perez-Gonzalez, P. G., et al. 2011, MNRAS, 417, 289
Bertone, S., & Conselice, C. J. 2009, MNRAS, 396, 2345
Bezanson, R., van Dokkum, P. G., Tal, T., et al. 2009, ApJ, 697, 1290

Binny, J., & Tremaine, S. 2008, in Galactic Dynamics, ed. J. Binney & S. Tremaine (2nd ed.; Princeton, NJ: Princeton Univ. Press), 34
Blakeslee, J. P., Holden, B. P., Franx, M., et al. 2006, ApJ, 644, 30
Bluck, A. F. L., Conselice, C. J., Almaini, O., et al. 2011, MNRAS, 410, 1174
Bluck, A. F. L., Conselice, C. J., Bouwens, R. J., et al. 2009, MNRAS, 394, 1956
Bridge, C. R., Carlberg, R. G., & Sullivan, M. 2010, ApJ, 709, 1067
Buitrago, F., Trujillo, I., Conselice, C. J., & Haeussler, B. 2011, MNRAS, submitted (arXiv:1111.6993)
Buitrago, F., Trujillo, I., Conselice, C. J., et al. 2008, ApJ, 687, 61
Cappellari, M., di Serego Alighieri, S., Cimatti, A., et al. 2009, ApJ, 704, L34
Carrasco, E. R., Conselice, C. J., & Trujillo, I. 2010, MNRAS, 405, 2253
Cenarro, A. J., & Trujillo, I. 2009, ApJ, 696, 43
Ceverino, D., Dekel, A., & Bournaud, F. 2010, MNRAS, 404, 2151
Cimatti, A., Cassata, P., Pozzetti, L., et al. 2008, A&A, 482, 21
Conselice, C. J. 2003, ApJS, 147, 1
Conselice, C. J. 2006, ApJ, 639, 120
Conselice, C. J. 2009, MNRAS, 399, 16
Conselice, C. J., Bershady, M. A., Dickinson, M., & Papovich, C. 2003, AJ, 126, 1183
Conselice, C. J., Bluck, A. F. L., Buitrago, F., et al. 2011a, MNRAS, 413, 80
Conselice, C. J., Bluck, A. F. L., Ravindranath, S., et al. 2011b, MNRAS, 1105, 2522
Conselice, C. J., Bundy, K., Trujillo, I., et al. 2007, MNRAS, 381, 962
Conselice, C. J., Rajgor, S., & Myers, R. 2008, MNRAS, 386, 909
Conselice, C. J., Yang, C., & Bluck, A. F. L. 2009, MNRAS, 394, 1956
Daddi, E., Cimatti, A., Renzini, A., et al. 2004, ApJ, 617, 746
Daddi, E., Renzini, A., Pirzkal, N., et al. 2005, ApJ, 626, 680
Daddi, E., Dickinson, M., Morrison, G., et al. 2007, ApJ, 670, 156
De Lucia, G., & Blaizot, J. 2007, MNRAS, 375, 2
De Propris, R., Conselice, C. J., Liske, J., et al. 2007, ApJ, 666, 212
De Vaucouleurs, G. 1948, Ann. Astrophys., 11, 247
Dekel, A., Birnboim, Y., Engel, G., et al. 2009, Nature, 457, 451
Elmegreen, D. M., Elmegreen, B. G., Yau, A., et al. 2011, ApJ, 737, 32
Fan, L., Lapi, A., De Zotti, G., & Danese, L. 2008, ApJ, 689, 101
Förster-Schreiber, N. M., Shapley, A. E., Genzel, R., et al. 2011, ApJ, 739, 45
Franx, M., Labbé, I., Rudnick, G., et al. 2003, ApJ, 587, L79
Grützbauch, R., Chuter, R. W., Conselice, C. J., et al. 2011a, MNRAS, 412, 2361
Grützbauch, R., Conselice, C. J., Bauer, A. E., et al. 2011b, MNRAS, 418, 938
Hopkins, P. F., Bundy, K., Murray, N., et al. 2009, MNRAS, 398, 898
Hopkins, P. F., Croton, D., Bundy, K., et al. 2010, ApJ, 724, 915
Hoyos, C., Aragón-Salamanca, A., Gray, M. E., et al. 2012, MNRAS, 419, 2703
Hubble, E. P. 1926, ApJ, 64, 321
Jogee, S., Miller, S. H., Penner, K., et al. 2009, ApJ, 697, 1971
Khochfar, S., & Burkert, A. 2006, A&A, 370, 902
Khochfar, S., & Silk, J. 2006, ApJ, 648, L21
Kitzbichler, M. G., & White, S. D. M. 2006, MNRAS, 366, 858
Lopez-Sanjuan, C., Balcells, M., Pérez-González, P. G., et al. 2010a, ApJ, 710, 1170
Lopez-Sanjuan, C., Balcells, M., Pérez-González, P. G., et al. 2010b, A&A, 518, 20
Lopez-Sanjuan, C., Le Fèvre, O., de Ravel, L., et al. 2011, A&A, 530, 20
Lotz, J. M., Davis, M., Faber, S. M., et al. 2008a, ApJ, 672, 177
Lotz, J. M., Jonsson, P., Cox, T. J., & Primack, J. R. 2008b, MNRAS, 391, 1137
Lotz, J. M., Jonsson, P., Cox, T. J., & Primack, J. R. 2010, MNRAS, 404, 575
Lotz, J. M., Jonsson, P., Cox, T. J., et al. 2011, ApJ, 742, 103
Man, A. W. S., Toft, S., Zirm, A. W., Wuyts, S., & van der Wel, A. 2011, ApJ, 744, 85
Mancini, C., Daddi, E., Renzini, A., et al. 2010, MNRAS, 401, 933
Metcalfe, N., Shanks, T., Weilbacher, P. M., et al. 2006, MNRAS, 370, 1257
Mortlock, A., Conselice, C. J., Bluck, A. F. L., et al. 2011, MNRAS, 413, 2845
Naab, T., Johansson, P. H., & Ostriker, J. P. 2009, ApJ, 699, L178
Newman, A. B., Ellis, R. S., Treu, T., & Bundy, K. 2010, ApJ, 717, L103
Onodera, M., et al. 2010, ApJ, 715, 60
Pannella, M., Carilli, C. L., Daddi, E., et al. 2009, ApJ, 698, 116
Papovich, C., Moustakas, L. A., Dickinson, M., et al. 2006, ApJ, 640, 92
Patton, D. R., Carlberg, R. G., Marzke, R. O., et al. 2000, ApJ, 536, 153
Peng, C. Y., Ho, L. C., Impey, C. D., & Rix, H. 2002, AJ, 124, 266
Rawat, A., Hammer, F., Kembhavi, A. K., & Flores, H. 2008, ApJ, 681, 1089
Ricciardelli, E., Trujillo, I., Buitrago, F., & Conselice, C. J. 2010, MNRAS, 406, 230
Thompson, R. I., Storrie-Lombardi, L. J., Weymann, R. J., et al. 1999, AJ, 117, 17
Trujillo, I., Conselice, C. J., Bundy, K., et al. 2007, MNRAS, 382, 109
Trujillo, I., Ferreras, I., & de La Rosa, I. G. 2011, MNRAS, 415, 3903
Trujillo, I., Förster Schreiber, N. M., Rudnick, G., et al. 2006, ApJ, 650, 18
van de Sande, J., Kriek, M., Franx, M., et al. 2011, ApJ, 736, L9
van Dokkum, P. G., Kriek, M., & Franx, M. 2009, Nature, 460, 717
van Dokkum, P. G., Rix, H.-W., Wuyts, S., et al. 2008, ApJ, 730, 38
Weinzirl, T., Jogee, S., Conselice, C. J., et al. 2011, ApJ, 743, 87
Yan, H., Dickinson, M., Eisenhardt, P. R. M., et al. 2004, ApJ, 616, 63